Tissue biomarkers for routine diagnostics and proteomic research in cutaneous melanoma malignum

Leticia Szadai M.D.

PhD Thesis

Szeged

2024

University of Szeged

Albert Szent-Györgyi Medical School

Doctoral School of Clinical Medicine

Tissue biomarkers for routine diagnostics and proteomic research in cutaneous melanoma malignum

PhD Thesis

Leticia Szadai M.D.

Supervisor: István Balázs Németh M.D. Ph.D.

Szeged,

2024

Table of contents

List of publications

Scientific papers included in this thesis:

I. Leticia Sz., Erika V., Beáta Sz., Natália P. de A., Gilberto D., Lazaro H. B., Jeovanis G., Matilda M.-V., Henriett O., Ágnes Judit J., Maria Del Carmen B.-A., Lajos K., Bo B., Johan M., Peter H., A Marcell Sz., István Balázs N., György M.-V. Deep Proteomic Analysis on Biobanked Paraffine-Archived Melanoma with Prognostic/Predictive Biomarker Read-Out. Cancers (Basel) (2021) Dec 3;13(23):6105. doi: 10.3390/cancers13236105. **IF:6.575** (Journal specialization: Scopus – Oncology, SJR indicator: Q1)

II. Leticia Sz., Jéssica de S. G., Nicole W., Natalia P. de A., Ágnes J., Ahmed R., Ferenc K, András K., Ede M., Guihong W., Nga N., Henriett O., Roger A., Fábio N., Gilberto D., Kun-Hsing Y., Yevgeniy R. S., Johan M., Melinda R., Elisabet W., David F., Lajos K., Peter H., István B. N., György M.-V., Jeovanis G., Mitochondrial and Immune Response Dysregulation in Melanoma Recurrence. Clinical and Translational Medicine. Clin Transl Med. 2023 Nov;13(11): e1495. doi: 10.1002/ctm2.1495. **IF: 7.9** (Journal specialization: Scopus – Medicine (miscellaneous), SJR indicator: D1)

Publications not directly related to the thesis:

III. István N.B., **Leticia Sz.,** Ágnes J.J., Zsuzsanna Ú., Tibor P., György M-V., Lajos K., Erika V., A molekuláris biológiai módszerek dermatopatológiai vonatkozásai. BŐRGYÓGYÁSZATI ÉS VENEROLÓGIAI SZEMLE, 2022, 98. ÉVF.3.152–158.DOI 10.7188/bvsz.2022.98.3.7.

IV. Erika V., **Leticia Sz.,** Qimin Z., Yonghyo K., Indira P., Aniel S., Roger A., Henriett O., Matilda M.-V., Boram L., Ho J. K., Johan M., Attila M. Sz., Jeovanis G., Lazaro H. B., István B. N., György M.-V. A biobanking turning-point in the use of formalin-fixed, paraffin tumor blocks to unveil kinase signaling in melanoma. Clin Transl Med. 2021 Aug;11(8):e466. doi: 10.1002/ctm2.466.

V. Lazaro H. B., Jeovanis G., Aniel S., Viktória D., Magdalena K., Jimmy R. M., Erika V., Uğur Ç., Yonghyo K., Yutaka S., Indira P. P., Beáta Sz., Roger A., Elisabet W., Charlotte W., Natália P. de A., Nicole W., Matilda M.-V., Jonatan E., Krzysztof P. , Bo B., Christian I., Håkan O., Lotta L., Henrik L., Henriett O., Boram L., Ethan B., Marie S., Carina E., Dasol K., Ho J. K., Beatrice K., Melinda R., Johan M., Runyu H., Peter H., A Marcell Sz., József T., Sarolta

K., Peter H., Tasso M., Toshihide N., Harubumi K., Erik S., Madalina O., Ken M., Francesco F., Quimin Z., Gilberto B D., Luciana P., Fábio C S N., **Leticia Sz.,** István B. N., Henrik E., David F., György M.-V. The Human Melanoma Proteome Atlas-Complementing the melanoma transcriptome. Clin Transl Med. 2021 Jul;11(7):e451. doi: 10.1002/ctm2.451. **IF:8.554** (Journal specialization: Scopus – Medicine (miscellaneous), SJR indicator: Q4)

VI. Lazaro H. B., Jeovanis G., Yonghyo K., Viktória D., Uğur Ç., Aniel S., Jimmy R. M., Magdalena K., Indira P. P., Yutaka S., Roger A., Elisabet W., Charlotte W., Erika V., Natália P. de A., Nicole W., Matilda M.-V., Krzysztof P., Jonatan E., Beáta Sz., Bo B., Christian I., Håkan O., Lotta L., Henrik L., Henriett O., Boram L., Ethan B., Marie S., Carina E., Dasol K., Ho J. K., Beatrice K., Melinda R., Runyu H., Peter H., Tasso M., Toshihide N., Harubumi K., Erik S., Madalina O., Ken M., Francesco F., Qimin Z., Gilberto B. D., Luciana P., Fábio C.S. N., Peter H., **Leticia Sz.,** József T., Sarolta K., Marcell A. Sz., Johan M., Dávid F., Henrik E., István N. B., György M-V., The human melanoma proteome atlas-Defining the molecular pathology. Clin Transl Med. 2021 Jul;11(7):e473. doi: 10.1002/ctm2.473. **IF:8.554** (Journal specialization: Scopus – Medicine (miscellaneous), SJR indicator: Q4)

VII. Leticia Sz., Aron B., Indira P. P., Alexandra L., Dorottya P., Anna S. L., Natália P de A., Ágnes J. J., Fábio N., Beata Sz., Viktória D., Nicole W., Jéssica G., Zsuzsanna U., Zoltán G. P., Tibor P., Yonghyo K., Balázs Gy., Bo B., Charlotte W., Marcell A. Sz., Lazaro B., Jeovanis G., Roger A., Ho J. K., Sarolta K., Magdalena K., Jimmy R. M., István B. N., Johan M., David F., Krzysztof P., Peter H., Elisabet W., Lajos V. K., Gilberto D., György M-V., Aniel S. Predicting immune checkpoint therapy response in three independent metastatic melanoma cohorts. Front. Oncol. 2024, 14:1428182. doi: 10.3389/fonc.2024.1428182. **IF:3.5** (Journal specialization: Scopus – Oncology, SJR indicator: Q2)

Abbreviations

ANT1, ANT2, ANT3: adenine nucleotide translocator-1,-2,-3

BAP1: BRCA1(breast cancer gene 1) associated protein 1

BRAF: B-raf proto-oncogene, serine/threonine kinase

CDKN2A: cyclin dependent kinase inhibitor 2A

cKIT: KIT proto-oncogene, receptor tyrosine kinase

COL4A2: collagen type IV alpha 2 chain

COL6A2: collagen type VI alpha 2 chain

HNRNPA1: heterogeneous nuclear ribonucleoprotein A1

ICAM2: intercellular adhesion molecule 2

ITGAX: integrin subunit alpha X

MC1R: melanocortin 1 receptor

MCAM: melanoma cell adhesion molecule, also known as CD146

MEK: mitogen-activated protein kinase kinase

MITF: melanocyte inducing transcription factor

mTOR: mammalian target of rapamycin

MTSS2: metastasis suppressor protein inverse Bin-Amphiphysin-Rvs domain containing 2

NRAS: neuroblastoma rat sarcoma virus, viral (v-ras) oncogene homolog

PSMB5: proteasome 20S subunit beta 5

PTEN: phosphatase and tensin homolog

SAMSN1: S-Adenosyl-L-methionine domain, Proto-oncogene tyrosine-protein kinase Src Homology 3 domain and nuclear localization signals 1

SNRNP70: small nuclear ribonucleoprotein U1 subunit 70

SNRPA1, B2: small nuclear ribonucleoprotein polypeptide A', B2

TERT: telomerase reverse transcriptase

TNFAIP2: tumor necrosis factor alpha induced protein 2

TP53: tumor protein 53

VEGFA - VEGFR pathway: vascular endothelial growth factor A and R pathway

1. Introduction

1.1. Management of melanoma malignum in patient care

Melanoma malignum (MM) is one of the most aggressive skin cancer with high metastatic potential, heterogeneous nature and is responsible for 80% of skin cancer-related deaths [1–3]. Melina Arnold *et al*. showed that whether 2020 rates persist, approximately 96 000 deaths (a 68% increase) and 510 000 new cases (a roughly 50% increase) will be estimated by 2040 [4]. Due to the unpredictable characteristics of disease course, it is a major clinical problem for the health care system accompanied by high treatment costs [5].

Among other skin cancer types, MM is the less frequent, however it is more aggressive and deadlier [5,6] than other skin tumors. The tumor derives from melanocytes which are specialized dendritic cells with neural crest origin. Melanocytes can be located in the epidermis of the skin, on mucosal surfaces, in the choroidal layer of the eye or in the meninges [5,7]. (The main focus of this thesis is cutaneous melanoma malignum.) The main function of melanocytes is the production of melanin by melanosome formation to protect the human skin from UV (ultraviolet) radiation [8–10]. Both genetic (e.g., familial dysplastic mole syndrome, mutations in MC1R, BAP1, TERT, MITF, PTEN, TP53, cKIT) and environmental factors (e.g., UV radiation) play pivotal role in the development of malignant melanoma.

In the management of melanoma, early diagnosis plays a crucial role. The initial step is the clinical detection of the suspicious lesion with using dermatoscopy[11] (**Figure 1**). Subsequently, surgical removal of the aforementioned skin lesion is undertaken, followed by a histology examination to determine the diagnosis (**Figure 1**).

Management of patients treated with melanoma
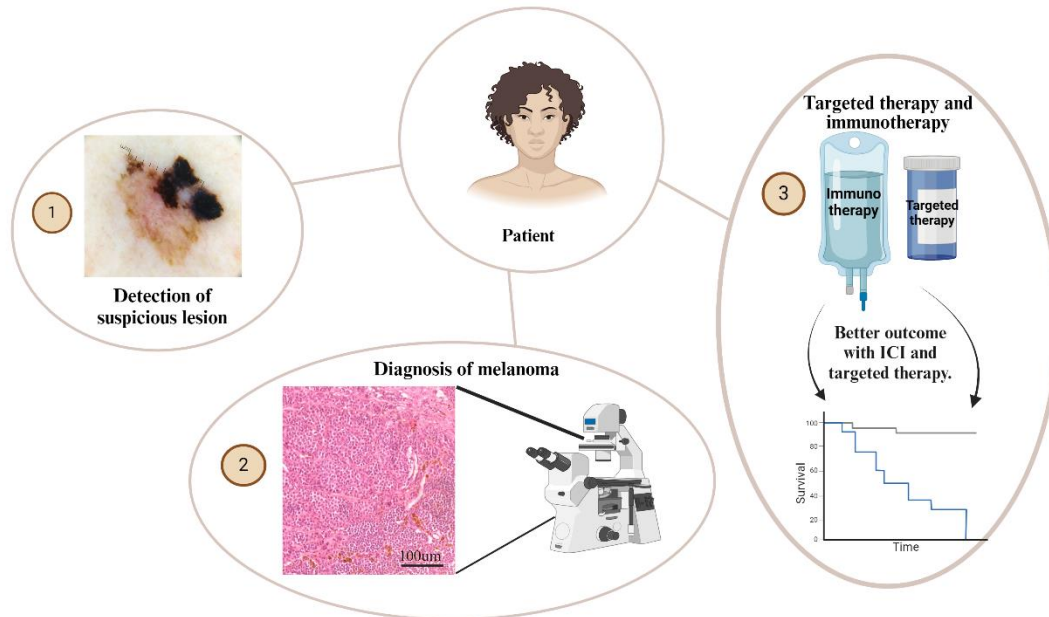
Figure 1 displays the main steps of management of melanoma patients including the detection of suspicious lesion by dermatoscopy (**1**), diagnosis of melanoma by histopathology (**2**), and the application of the adequate therapy (e.g., targeted therapy and immunotherapy) (**3**). The images of dermoscopy and histology were collected in the Department of Dermatology and Allergology, University of Szeged. (ICI – immune checkpoint inhibitors, OM 112x, scale bar 100 μm)

According to the European consensus-based interdisciplinary guideline for melanoma, histopathology validation differentiates 4 main primary melanoma subtypes: nodular, superficially spreading, acral lentiginous and lentiginous melanoma maligna[11]. Beyond the main types, additional subtypes such as desmoplastic, mucosal, uveal, spitzoid, amelanotic melanoma have been identified[11,12]. Different histopathology features provide additional information about the tumor morphology such as the Clark level (reflecting level of invasion)[11], the Breslow level (indicating vertical tumor thickness)[11], type of the melanoma cells (e.g., epithelioid, spindle-shaped cells etc.)[13], pagetoid spreading especially in SSM[13], ulceration [11], regression (e.g., host tissue response)[11], mitotic rate (number of mitosis/mm^2)[11], the detection of tumor-infiltrating lymphocytes, or microsatellite metastases (e.g., satellite, in-transit or micro-metastases)[11] (**Figure 2**).

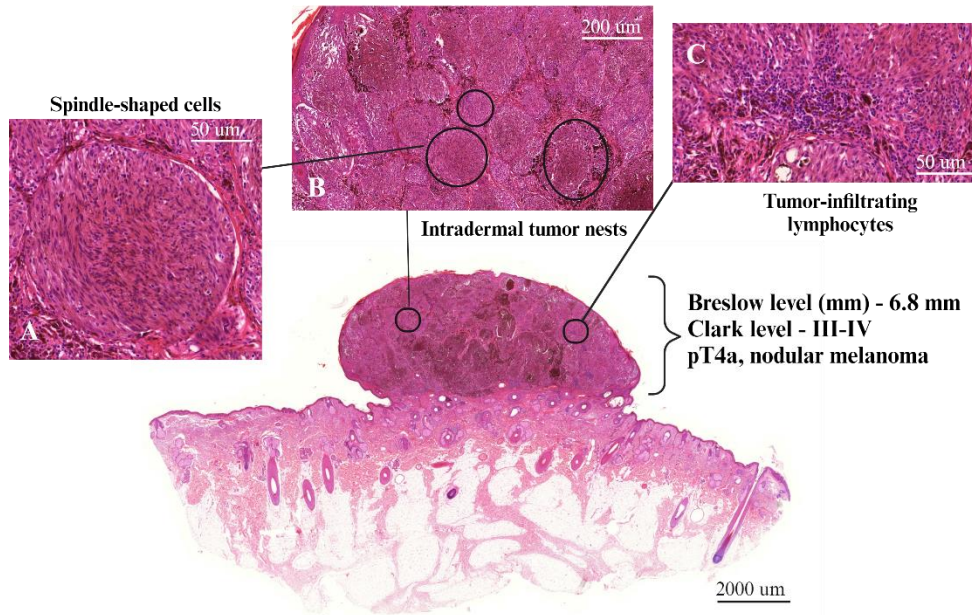**Figure 2** shows a representative H&E image of a nodular melanoma with histopathology features indicative of tumor spreading. Image **(A)** presents spindle-shaped cells, common feature in nodular melanoma[13]. Image **(B)** displays the intradermal tumor nests indicative of vertical growth, and image **(C)** depicts tumor-infiltrating lymphocytes correspond to immune response. The H&E image was obtained in the Department of Dermatology and Allergology, University of Szeged. (OM 112x, scale bar from 50 μm to 2000μm)

In the routine diagnostics, additional immunohistochemistry staining provides more information to detect the melanoma cells (e.g., S100B (S100 calcium binding protein B), HMB45 (Human Melanoma Black – 45), Ki-67 protein (marker of proliferation Ki-67), SOX10 (SRY-box transcription factor 10), Melan-A (melanoma antigen recognized by T cells, also known as MART-1 antigen), and in special cases BRAFV600E (for mutated Braf kinase)[14]. Prior to the initiation of melanoma therapy, it is essential to detect both locoregional and distant metastases, and consequently to determine the clinical staging of the patient based on the current melanoma staging guideline: The American Joint Committee on Cancer eighth edition (AJCC8) [15].

Regarding the therapy options, the application of kinase and immune checkpoint inhibitors have revolutionized the management of melanoma in the last 10 years. Several studies demonstrated the effectiveness of both targeted and immunotherapies, indicating an increase in the survival rate for patients receiving these therapies[11](**Figure 1**). The main two therapy options have different molecular mechanisms for the antitumor activity. The FDA-approved targeted therapies (e.g., dabrafenib, trametinib, vemurafenib, cobimetinib, encorafenib, binimetinib),

administered based on the BRAF mutation status, inhibit cell proliferation by blocking the increased activation of Braf and Mek kinases. The FDA-approved immunotherapies such as inhibitors of CTLA-4 (cytotoxic T-lymphocyte associated protein 4, e.g., ipilimumab), LAG-3 (lymphocyte-activation gene 3, e.g., relatlimab), PD-1 (programmed cell death protein 1, e.g., nivolumab, pembrolizumab) and PD-L1 (programmed cell death ligand 1, e.g., atezolizumab) are recommended for all individuals with unresectable metastatic melanoma irrespective from tumor BRAF mutation status[11]. The immune checkpoint inhibitors hinder the connection between lymphocytes and tumor cells by blocking the T cell surface proteins and it facilitates the activation of lymphocytes to eliminate the tumor cells[5,16]. These mechanisms have also an effect on melanoma microenvironment[2]. Beside the effectiveness of these biological treatments, the rapid development of therapy resistance and toxicity (e.g., immune-related adverse effects (irAE)) is a prevalent problem during the administration of these therapies.

1.2.   Role of prognostic and predictive biomarkers

When discussing biomarkers, it's important to highlight the increasing significance of proteins. In diseases and cancers, proteins play a central role in predicting outcomes. For instance, higher expression of autoantibodies can indicate disease activity in autoimmune diseases[17], while certain proteins (e.g., C-reactive protein) can point to an inflammation in the body[18]. Proteins such as prostate-specific antigen help detecting small, low-grade, localized prostate cancers[19], and high level of thyroglobulin levels can predict the recurrence of thyroid tumors after thyroid gland removal[20]. Therefore, proteins can serve as a basis for prognostic and predictive approaches.

In the case of melanoma malignum, the high tumor mutational burden (TMB) [21–23] involves numerous pathways and proteins in tumor formation. In the last decade, promising results have emerged from analyzing various biomarkers for disease progression. These include the blood level of lactate dehydrogenase (LDH)[23,24], mutations in genes (e.g., MITF[low/high], CDKN2A)[23,25], influence of immune cells (e.g., high density of CD3+/CD8+ T lymphocytes, CD20+ B cells [23,26,27]), as well as ulceration and mitotic rate. However, they lack standardization and accuracy in predicting outcomes. At present, the determination of Breslow level and the status of sentinel lymph nodes form the basis for the current melanoma staging[15], but there is a need for more accurate and comprehensive prognostic biomarkers at the molecular level.

In the histopathology of melanoma, biomarkers can be categorized based on their functions, including prognostic biomarkers for predicting the disease progression, and predictive biomarkers for anticipating therapy response[14]. The BRAF mutation is a major predictive target, present in about half of melanocytic lesions and typically occurring early in tumor development. In 80-90% of the cases, BRAF mutations are in the V600 position when valine substitute to glutamate resulting in the V600E mutation. Other mutations are also known like V600K, V600R and V600D. BRAF mutations occur in sun-exposed locations of the skin[5], and has a pivotal role in treatment choice. Currently, the gold standard method for the mutation detection is DNA-based PCR (polymerase chain reaction) analysis[28]. During the polymerase chain reaction analysis, the targeted gene is amplified to ascertain whether the mutation is in the sample[28]. The DNA-based techniques are time-consuming, expensive, and require comparison with histology findings to avoid cross-contamination[29]. Technical factors like melanin's inhibitory effect and low tumor content can lead to false results[30–32]. Protein-based immunohistochemistry (IHC) staining is an emerging alternative for detecting BRAF mutations. Although the protein-based immunohistochemistry (IHC) staining is not yet part of the routine diagnostics, it is cost-effective and suitable for healthcare settings[33]. It utilizes the VE1 clone antibody which is specific for BRAFV600E mutated protein. For the staining method, one layer from the formalin-fixed paraffin embedded (FFPE) tumor sample is sufficient[34]. Twenty percent of tumor content is adequate to detect the abnormal protein[35]. It was also demonstrated that the protein is well-preserved during IHC staining process, unlike PCR analysis[36]. Furthermore, demonstrating the presence of mutated proteins during IHC diagnostic method is beneficial for therapy choice, as targeted therapy works by inhibiting the BRAF kinase proteins. In addition, immunohistochemistry staining of BRAF mutated protein is a predictive tool not only for melanoma but also for colorectal cancer and thyroid cancer[37]. This thesis will present the results of the comparison of the two methods with complementary analyses.

Concerning therapy response, melanoma is recognized as immunogenic, exhibiting higher immune cell infiltration compared to other tumor types. Due to the tumor mutation burden[38–40], there is an increased likelihood of producing mutant proteins, which can serve as neoantigens, thereby enhancing immunogenicity[21,23,41]. In contrast, almost half of melanoma patients either do not respond to immune therapy or progress due to resistance[5,42]. Currently the mechanisms behind therapy resistance is not fully understood. Studies on the proteomic and histopathology characteristics of melanoma samples have aimed to enhance the prediction of immunotherapy

response. For instance, it is known that tumor-infiltrating lymphocytes (TIL) are crucial for immunotherapy response [5,27,43–45]. In addition, macrophages can adopt either anti-tumor (M1) or pro-tumor (M2) roles depending on TME signals, potentially impacting the progression and later the treatment outcomes[5,46]. Based on the function of tumor-infiltrating lymphocytes, a new FDA approved cellular therapy named Lifileucel® (Amtagvi) has recently been introduced with promising outcomes. This therapy promotes the TILs of the tumor of the patient to booster immune activity against tumor cells[47]. Current publications indicate that the combination of PD-L1 cell type expression with tissue localization can have clinical significance[48]. However, relying on a single marker to predict treatment response has limitations[5]. There remains an unmet need for identifying biomarkers that distinguish responders from non-responders to immune checkpoint inhibitor therapy.

Regarding prognostic approaches, under the umbrella of artificial intelligence (AI) in digital pathology, several studies have attempted to find features indicative of progression of melanoma [49,50]. Wan *et al.* developed a machine-learning algorithm with 36 clinicopathologic features to predict the recurrence risk[51]. They highlight the predictive attributes of mitotic rate and Breslow tumor thickness[51]. Moreover, Kulkarni *et al.* utilized deep learning convolutional neural networks (CNN) to predict disease-specific survival from 263 melanoma H&E slides[52]. Furthermore, a novel computational method, the Estimate Systems Immune Response score (EaSIeR)[53], has emerged which predicts immunotherapy response in cancer patients by analyzing tumor microenvironment signatures and 14 transcriptome-based immune response indicators[53]. Our research group utilized this approach to identify proteins distinguishing responders from non-responders. Six proteins (ITGAX, SAMSN1, TNFAIP2, CD163, MTSSS2, and PSMB5) from an immunotherapy-treated cohort were correlated with therapy response. These proteins were validated in two untreated cohorts. In addition, among these proteins, three (ITGAX, TNFAIP2, and SAMSN1) were associated with patient survival at both protein and transcript levels in an independent immunotherapy-treated cohort. These 6 proteins were linked to different pathways of the tumor microenvironment. For instance, ITGAX is a cell adhesion molecule involved in integrin binding[54]; SAMSN1 plays role in regulating B cell activation[55]; TNFAIP2 is a cancer-related gene, pivotal in inflammation[56,57]; CD163 is an acute phase-regulated receptor crucial for shielding tissues from oxidative damage caused by free hemoglobin[58]; and MTSS2 contributes to plasma membrane dynamics[59,60]. The results highlight that AI is an emerging approach in the prediction of immunotherapy. However, beside the results so far, AI still faces limitations and numerous challenges[49].

Moving forward to other approaches, tissue samples such as FFPE samples emerges as a cornerstone in tissue-based biomarker research. For histopathology evaluation, FFPE sections serves to deepen our knowledge of the tumor morphology and the tumor microenvironment as well as their connections. Combining histopathology with different OMICS platform analyses (genomics, transcriptomics, proteomics)[61], FFPE samples may become a key element in extending knowledge of tumor molecular fingerprints. In 2021, our research group in a wide international cooperation, pioneered the publication of a comprehensive proteomic fingerprint and morphological analysis of 500 melanoma samples through complex OMIC approaches[62]. Additionally, another study performed a comprehensive proteogenomic comparison with a specific focus on possible driver-, and therapy-associated genes in melanoma[63]. These advancements underscore the vast possibilities that proteomics analysis offers for predictive and prognostic biomarker research, with potential implementation in patient care through combined histopathology evaluation.

In this thesis, we will present our results using innovative approaches such as quantitative proteomics and digital pathology with AI-driven imaging to aim spatial proteomics. Our advancements in biomarker research provide a deeper understanding of the molecular features of melanoma, holding promise for more personalized treatment approaches and ultimately improving patient outcomes.

.

2. Aims

Our research group is dedicated to uncover proteins from paraffin-archived melanoma samples for predictive and prognostic purposes with novel methodologies. In the scope of this discovery project, our goals are the following (**Figure 3**):

- To compare the use of PCR technique and IHC staining on BRAF mutation detection in routine diagnostics.
- For predictive purposes, we conduct a comprehensive proteomic analysis on FFPE melanoma samples to unveil potential proteins predicting therapy outcomes.
- For prognostic purposes, we introduce an AI-powered digital pathology approach alongside an in-depth quantitative proteomics analysis of 12 early-stage primary melanomas to detect potential proteins predicting progression.
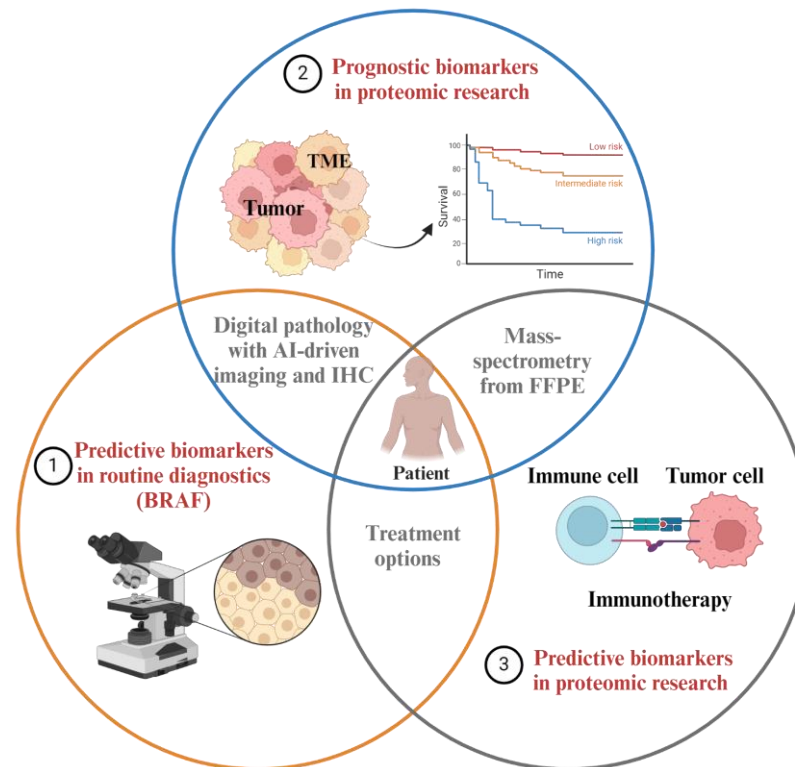
Figure 3 summarizes the different approaches and objectives of our melanoma biomarker research, with personalized medicine at the core. Our studies aimed to identify biomarkers with predictive and prognostic purposes in routine diagnostics (**1**) and in proteomic research (**2,3**) for melanoma using spatial proteomics, including the combination of digital pathology with AI-driven imaging (**2**), immunohistochemistry (IHC) (**1**), and quantitative proteomics (**2,3**).

3. Materials and Methods

Based on the BRAF detection study, the predictive biomarker study **(paper I)** and the prognostic biomarker study **(paper II)**, here I summarize the materials and methods of these studies.

3.1. Workflow of the studies involved in the thesis

3.1.1. The workflow of the BRAF detection study

In the initial step of our BRAF detection study, we collected 94 formalin-fixed paraffin-embedded melanoma samples along with their clinical data (**Figure 4, 1**), including PCR data of BRAF mutations (**Figure 4, 2**). These samples were then stained with VE1 antibody for BRAF mutation (**Figure 4, 2**). Samples that were PCR-negative for BRAF mutations but showed focal positive staining were submitted for next-generation sequencing (**Figure 4, 3**). Samples that were PCR-negative for BRAF mutations but showed diffuse positive staining with intratumoral heterogeneity were sent for quantitative PCR (**Figure 4, 3**). The methodology steps are detailed in 3.2 to 3.8 paragraphs.
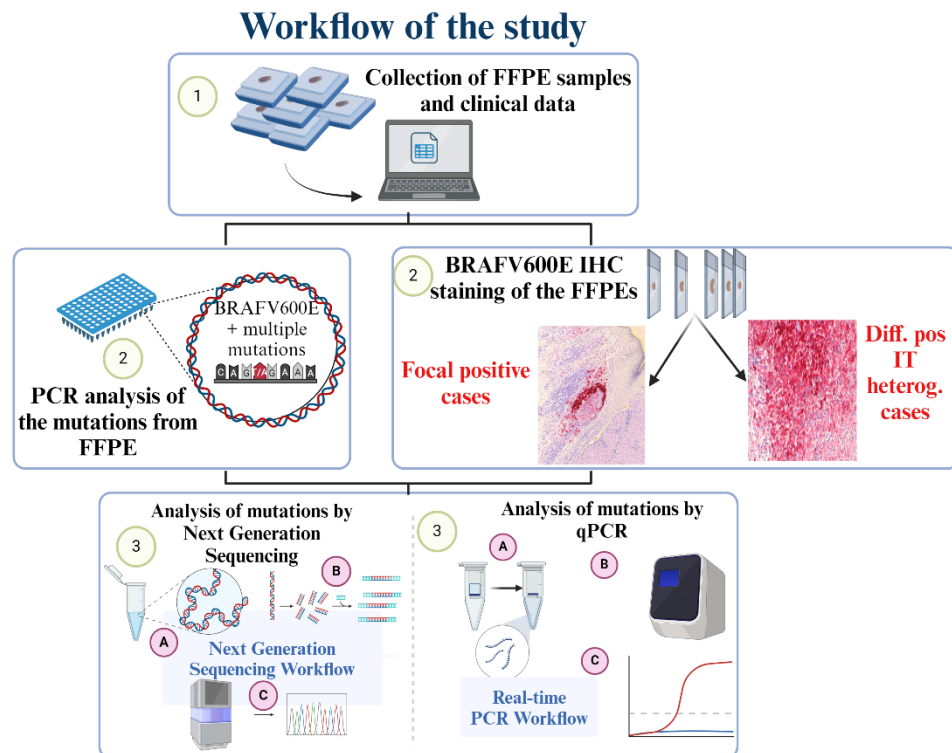

Figure 4 shows the workflow of the BRAF detection study. It captures the different approaches utilized for BRAF mutation detection in the study (**1-3**). /Diff.-diffuse, pos. – positive, IT -intratumoral/

3.1.2. The workflow of the predictive biomarker study (paper I)

This study encompassed 90 formalin-fixed paraffin-embedded melanoma samples collected retrospectively during oncology care and follow-up[64]. Detailed clinical information was collected for each sample. These archived melanoma samples were then subjected to histopathology analysis to obtain histopathology description from the samples. Moreover, the melanoma samples were sent for proteomic analysis using high-resolution mass spectrometry[64] (**Figure 5**). The methodology steps are detailed in 3.2 to 3.8 paragraphs.
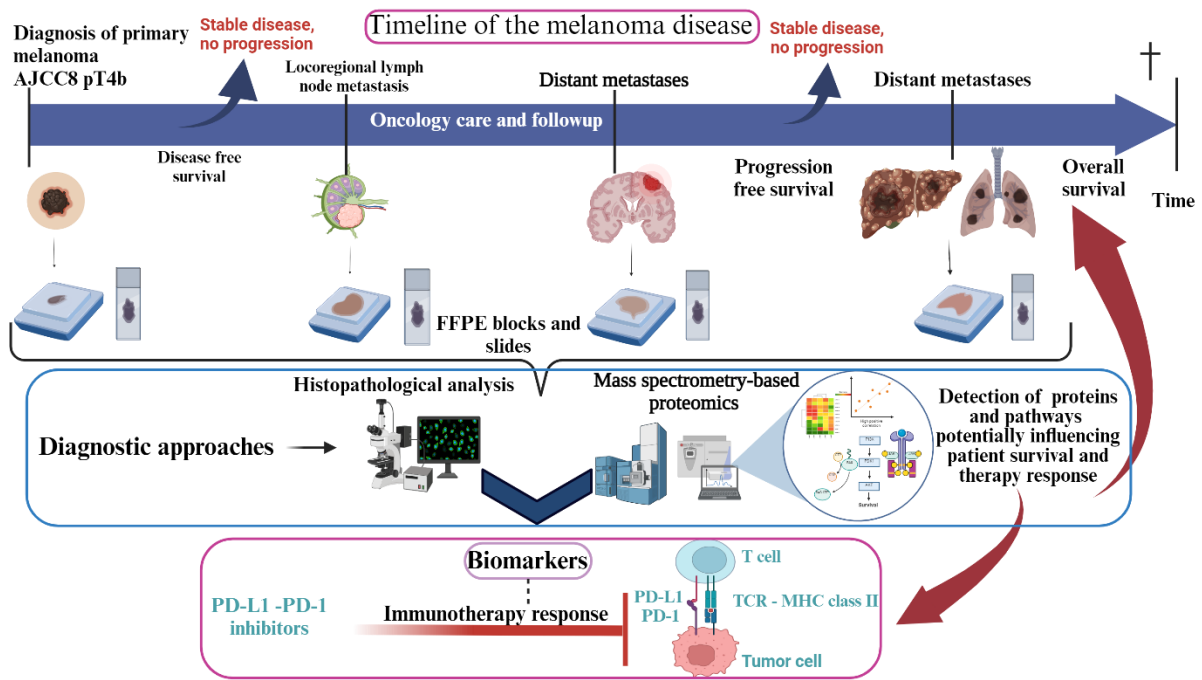

Figure 5 illustrates the general workflow of our predictive biomarker study, presenting the timeline of melanoma disease progression from tumor diagnosis to the development of distant metastases. It also outlines the main steps for obtaining data from archived formalin-fixed paraffin-embedded melanoma samples, including proteomic analysis[64].

3.1.3. The workflow of the prognostic biomarker study (paper II)

The study involves six early-stage formalin-fixed paraffin-embedded melanoma samples with recurrence, and six without recurrence. Initially, the formalin-fixed paraffin-embedded melanoma samples were sectioned and H&E stained for histopathological investigation combined, with topographic image analysis based on artificial intelligence (AI). With the help of data-rich imaging, deep-learning, and machine-learning models, a digital pathology profile was set up to automatically identify and annotate tumor and stromal areas. The sections with annotated regions were subjected to laser capture microdissection (LCM) to isolate and collect tumor and stromal cells for quantitative proteomics. A recently implemented sample preparation workflow (see detailed in paragraph 3.6 in Materials and Methods[61,65]) was used to achieve deep proteome profiling of all 24 samples with mass-spectrometry[66]. Finally, bioinformatics analysis and biological interpretation of the proteomic data were conducted (**Figure 6**).
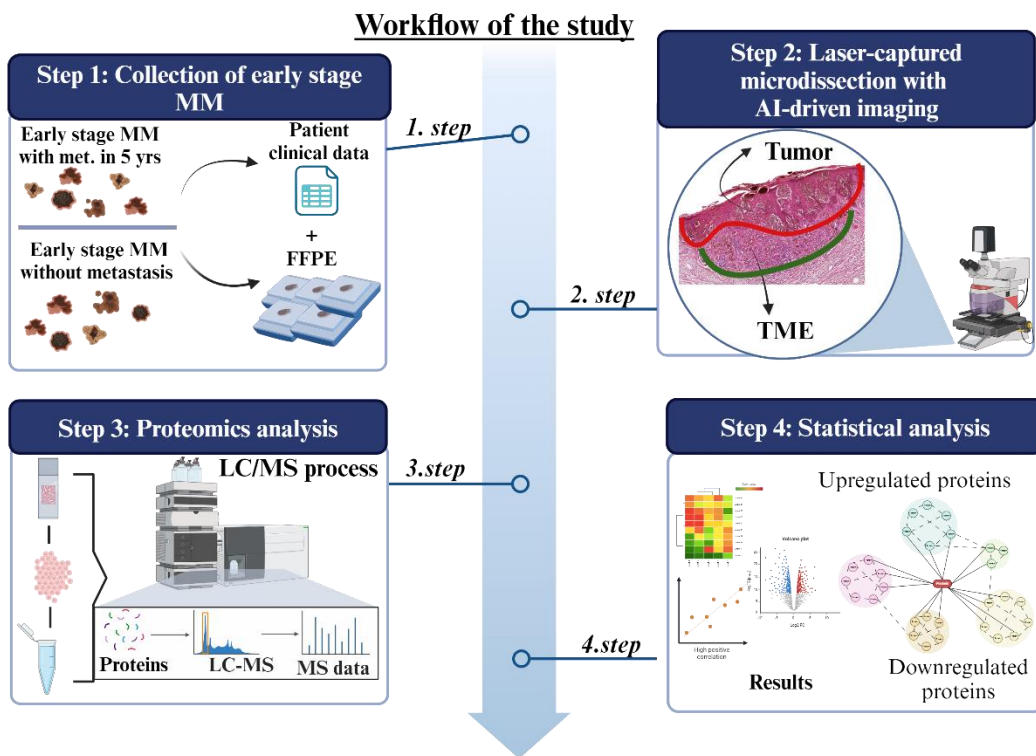

Figure 6 summarizes the main steps of our prognostic biomarker study. This includes the collection of early-stage formalin-fixed paraffin-embedded melanoma samples, the process of the laser capture microdissection with AI-driven imaging, proteomic analysis and statistical analysis of the samples[66]. /LC/MS - liquid chromatography–mass spectrometry/

3.2. Patient cohorts

In the BRAF detection study, a total of 94 melanoma samples were collected retrospectively from 94 patients in the Department of Dermatology and Allergology of the University of Szeged. The inclusion criteria for this study involved patients whose melanoma samples had been archived in formalin-fixed paraffin-embedded (FFPE) tissue blocks and had undergone BRAF mutation analysis using PCR detection and BRAF immunohistochemistry staining. The samples were collected with clinical information including gender, age at primary melanoma, clinical staging, survival data, therapy received, melanoma subtypes, histological parameters of the tumor (**Table 1**).

Clinical and histopathologic characteristics of the samples			
Tumor type *(N)*		**Clinical staging based on AJCC8** *(N)*	
Prim	91	IA	1
Met	3	IB	4
Age at primary		IIA	7
Mean	62.7 yrs	IIB	10
SD	± 5.65	IIA/IIB	1
Sex *(N)*		IIC	8
Male	60	IIIA	6
Female	34	IIIB	7
Primary melanoma type *(N)*		IIIC	37
SSM	12	IIID	3
SSM with vertical growth	32	IV	9
NM	30	NA	1
Malignant blue nevus	1	**Breslow level (mm) of primary melanoma**	
LMM	1	< 1.00	5
ALM	10	1.01-2.00	13
ALM with vertical growth	1	2.01-4.00	29
Epitheloid melanoma	2	4.01 <	42
Melanoma residuum	1	no data	2
NA	1		
Ulceration *(N)* **of primary melanoma**			
yes		57	
no		32	
no data		2	
Received therapy *(N)**			
No therapy	Targeted therapy	Immunotherapy	Other therapy (INF, ECT, RadioT, ChemoT)
24	17	43	35

Table 1 shows the clinical and histopathologic parameters of the samples included in the BRAF detection study. *Patients received more than a single therapy. /N-number, Prim – primary, Met – metastasis, SD – standard error, ALM- acrolentiginous melanoma, LMM-lentigo maligna melanoma, NM-nodular melanoma, SSM-superficial spreading melanoma, lymph. – lymph node metastasis, cut. – cutaneous metastasis, INF – interferon therapy, ECT – electrochemotherapy, RadioT – radiotherapy, ChemoT – chemotherapy, NA – no data available, AJCC8 – The 8th edition of American Joint Committee on Cancer Staging System/

The predictive biomarker study, refers to **paper I**, included 52 patients with primary and 25 patients with metastatic melanoma collected from the Department of Dermatology and Allergology at the University of Szeged, analyzing 53 primary and 37 metastatic melanoma samples. The patients were selected retrospectively from 2005 to 2020, with primary melanoma or metastasis archived in formalin-fixed paraffin-embedded tissue blocks. All primary tumors resulted in loco-regional and/or disseminated disease. The histopathological slides were prepared from formalin-fixed, paraffin-embedded (FFPE) blocks, collecting a total of 90 samples with clinical information, including gender, age at primary tumor (in 3 cases the age at primary was not available), age at metastasis, age at collection date, localization of primary tumor and metastases, long-term follow up data of the patients: disease-free survival (DFS), progression-free survival (PFS), overall survival (OS) (in 3 cases the DFS, PFS and OS were not available), AJCC8 clinical staging, histological parameters of the primary tumor, mutational status, therapies received. Disease-free survival (DFS), progression-free survival (PFS), and overall-survival (OS) were calculated based on the date of clinical diagnosis of the primary melanoma to the date of first metastasis, progression, and death or last follow-up, respectively (**Table 2**). Detailed clinical, histopathologic data and the survival analyses are available in the publication by Szadai L. *et al.*[64].

Number of the patients	Tumor samples (n =90)		Type of primary tumors (N)	
77	Primary tumors	53	SSM with vertical growth	15
	Locoregional lymphatic metastases	24	SSM	5
Clinical stage (AJCC8)	Cutaneous metastases	13	NM	27
			ALM	3
St. I. 7 patients	**Disease-free survival***		ALM with vertical growth	1
St. II. 24 patients			ALM with SSM	1
St. III. 31 patients	17 months	0-45 months	LMM	1
St. IV. 14 patients	**Progression-free survival***		**Therapies of the patients (N)**	
NA 1 patient	42 months	3 - 81 months	Immunotherapy	22
Age at primary*	**Overall survival***		Targeted therapy	15
mean range	51 months	6 - 96 months	Other therapies (irradiation, ETC, chemotherapy, INF therapy)	59
64 yrs 54-74 yrs				
			No therapy	18

Table 2 displays the clinicopathologic data of the patient cohort of paper I. The table displays the clinicopathologic parameters of the patients and their selected primary melanomas and metastases included in the metastatic patient cohort. /SSM-superficial spreading melanoma, LMM-lentigo maligna melanoma, NM-nodular melanoma, ALM-acrolentiginous melanoma, St. – status, AJCC8 – The 8th edition of American Joint Committee on Cancer Staging System, yrs - years, NA – no available data./. *Data were not available in three cases.

The prognostic biomarker study, refers to **paper II**, incorporated twelve patients with cutaneous primary melanoma after presenting with their lesion to the Department of Dermatology and Allergology at the University of Szeged between 2006 and 2017. The FFPE blocks of primary melanoma samples were collected retrospectively. Clinicopathological data including age,

gender, clinical stage, histopathological subtype, histological parameters of the primary tumor, and survival parameters (DFS, PFS, and OS) are detailed in Szadai *et. al.* [66]. The calculation of DFS, PFS, and OS were delineated above. The primary tumor samples were categorized into two groups: one from patients who experienced disease recurrence within 5 years after the initial diagnosis (Group B, n=6), and the other from those patients without metastatic events within that same 5-year period (Group A, n=6). All these tumor samples were from the early stages of the disease, specifically classified as AJCC8 IA-IIA at diagnosis. For both groups, survival parameters were calculated from the date of primary melanoma diagnosis to the date of the last follow-up (**Table 3**).

CLINICOPATHOLOGICAL PARAMETERS		Non-recurrent (Group A, n=6)	Recurrent (Group B, n=6)
Patients	**Variable**	**Median ± SD**	**Median ± SD**
Age	**Age at primary diagnosis (years)**	68 ± 8.7	61 ± 16
Survival	**DFS (m)[1]**	89 ± 18	49 ± 13
	PFS (m)[2]	89 ± 18	60 ± 10
	OS (m)[3]	89 ± 18	61 ± 22
Breslow level	**Breslow level (mm)**	0.23 ± 0.1	1.21 ± 0.4
Patients	**Variable**	**Patient (n) /Total (n)**	**Patient (n) /Total (n)**
Gender	**Male**	6/6	2/6
	Female	0/6	4/6
Clinical stage (AJCC8)	**IA**	6/6	2/6
	IB	0/6	3/6
	IIA	0/6	1/6
Type	**SSM[4]**	6/6	6/6
Clark level	**II**	6/6	1/6
	III	0/6	5/6
Regression	**Presence of regression areas**	6/6	3/6
Ulceration	**-**	0/6	3/6

Table 3 represents the clinical and histopathological features within recurrent and non-recurrent groups of primary melanomas. Median and standard deviation (SD) are represented for continuous variables, and number of patients (n) are shown for categorical variables. [1]DFS: disease-free survival, [2]PFS: progression-free survival, [3]OS: overall survival, [4]SSM: superficial spreading melanoma. /m- months, mm- millimeter/

3.3. Molecular analysis in the BRAF detection study
3.3.1. Routine polymerase chain reaction (PCR) with Sanger Sequencing

The FFPE samples underwent analysis for BRAF V600 mutations using the DNA-based Sanger Sequencing technique. DNA isolation was carried out from the FFPE samples of both primary melanomas and metastases at the Department of Pathology, University of Szeged. Prior

to the DNA-based analysis, the assessment of the ratio between melanoma and reactive/healthy cells was performed, and samples with a minimum 80% melanoma cells were eligible for the analysis. During the PCR process, the hotspots of the BRAF gene mutation were amplified, and the resulting gene products were sequenced. Besides testing mutations of the BRAF gene (V600E, V600K, V600R, K601E mutations), cKIT gene was also successfully amplified and detected.

3.3.2. Next generation sequencing (NGS) – DNA extraction, library construction, data processing, variant calling

From the stained slides, the target regions for the molecular genetic investigation were selected by a pathologist. Genomic DNA was extracted from the 9 FFPE tissue samples using the MagCore® Super nucleic acid isolation robot, Genomic DNA FFPE One-Step Kit (RBC Bioscience Corp., Taiwan). The elution volume was 60 ul. Subsequently, BRAF exon 15, potentially harboring the V600E mutation, was amplified by PCR from the purified FFPE DNA. The PCR amplification was carried out in a reaction volume of 30 ul using 5 pmol of each primer (region of interest: 7:140753268-7:140753365), the sequences of the oligos, used in the first PCR are the following: forward primer 5'-GCGACGCACACAGCACGCGCAGNNNNNNNNNNNNNNAATACGTCGATTGCCATCAG TGGAAAAATAGCCTCAA-3', reverse primer 5'-GGCAACCGCCGTGTTGGAGGCCNNNNNNNNNNNNNNTGCTTTGTACGTAGCTCATG AAGACCTCACAGT-3', 1x Q5 Reaction Buffer, 0.6 U Q5 High-Fidelity DNA Polymerase (New England Biolabs, Ipswich, MA, USA), 200 μM of each deoxynucleotide, 10.6 ul AccuGene water (AG; Lonza, Basel, Switzerland) and 10 ul isolated DNA of each FFPE samples. A positive control was established using a serial dilution of previously identified BRAF mutant formalin-fixed paraffin-embedded (FFPE) samples, while AG served as a negative control. Thermal cycler conditions were as follows: 98 degrees Celsius for 45 sec, 45 cycles of 15 sec at 98 degrees Celsius and finally, 45 sec at 62 degrees Celsius. Amplification quality control was conducted by running the reactions on a 3% agarose gel.

The amplicons underwent purification using the KAPA Pure Bead (Roche, Basel, Switzerland) with a volume ratio of 0.8 between beads and PCR products. The purified products were eluted in 16 ul AG. Indexing PCR was performed in 20 ul using 1 pmol of each primer (containing Nextera XT Sequencing Adapters), 1x Q5 Reaction Buffer, 0.4 U Q5 High-Fidelity DNA Polymerase (New England Biolabs, Ipswich, MA, USA), 200 μM of each deoxynucleo-tide, 4.5 ul AG and 8 ul amplicon. The temperature profile consisted of an initial step at 98 degrees

Celsius for 1 min, followed by 15 cycles of 15 sec at 98 degrees Celsius and 50 sec at 63 degrees Celsius. Nextera XT sequencing adapters were extended with the sequence and the seven intermediate nucleotides. Additionally, to enhance diversity in the amplicon library, each i5 sequencing adapter was used as a pool of four primers in which a 'N' (0-3) spacer was added between the Ilumina sequencing primer and sequence.

DNA quality and correct sizing were monitored through nested PCR using 5'-6-FAM-labeled primers for a fragment analysis on the 3500 Genetic Analyzer (Applied Biosystem Foster City, CA, USA). The dual-indexed library products underwent purification in the same manner as the products of the first PCR round, and they were purified in 12 μl AG as well. Quantification of the sequencing libraries were performed using the Qubit quantification method (Invitrogen, Carlsbad, CA) with the Qubit dsDNA High-Sensitivity Assay Kit (Life Technologies, Carlsbad, CA). Subsequently, after pooling at equimolar ratios, the DNA library was sequenced on an Ilumina NextSeq 550 System using the NestSeq 500 High-Output Kit v2.5.

The data processing and variant calling followed the methodology outlined by Priskin *et al.*[67]. The first filter level was determined by low Q values, allowing a maximum of 30 bases below Q28 in both R1 and R2 directions for a read pair, resulting in 0.5-1% of the reads filtered out. In the second filter level 33-50% of the reads were filtered out, because only the perfectly aligned read pairs were accepted, facilitated by our primer design, resulting in a product shorter than base pairs [68]. Finally, in the third filter level, we eliminated primers from the ends of the readings using the Smith – Waterman algorithm based on the primer list, allowing a 3-base Hamming distance, particularly significant for overlapping primer pairs. The last filter level used the UMI tools[69] and UMI sequences at end to cluster all reads with the same UMI, removing all read clusters that had more than one read. Mutation selection criteria included coverage of >10000 and a frequency of mutated alleles >1.5% for target reads. Clinical significance was annotated using SnpSift on the dbSNP and Clinvar variant database. The NGS was carried out in the Biologic Research Centre in Szeged.

3.3.3. Real-time polymerase chain reaction (qPCR) - qPCR quantification of the patient samples

For each quantification, the tumor part of 4 μm thin samples was selected based on evaluation of a pathologist and utilized for further isolation. DNA isolation was performed using the ReilaPrep FFPE qDNA Minimprep kit (#A2352 Promega, USA), following the manufacturer's instructions. BRAF V600E and V600D mutated alleles were identified using qRT-PCR detection with the gb ONCO BRAF (V600E) CE-IVD kit (3241-024, Generi

Biotech, Czech Republic). Ct values were measured and analyzed on the Applied Biosystems QuantStudio 5 platform (Thermo Fisher Scientific, USA). The cycler temperature profile and running mode were adjusted as specified in the detection kit. Mutation statuses were calculated and determined using the batch-compatible evaluation table (EC_SOMMUT ver 1.4) provided by the manufacturer. The qPCR was performed in the Department of Pathology, University of Szeged.

3.4. Immunohistochemistry validation

In the BRAF detection, predictive **(paper I)** and prognostic biomarker studies **(paper II)**, retrospectively collected samples were obtained through excision or biopsy of primary melanoma or metastatic organs, following routine formalin-fixed and paraffin-embedded (FFPE) methodology for archival purposes. In the BRAF detection and the predictive biomarker study **(paper I)**, the FFPE tissues were underwent stepwise sectioning with a conventional microtome, adjusted to a slice thickness of 4 micrometers. In the prognostic biomarker study **(paper II)**, the examined formalin-fixed paraffin-embedded tumor samples incorporated a range of thickness from thin, low risk (< 1 mm, pT1a) – characteristic of the no recurrence subgroup, to medium thick, medium risk (1–1.6 mm, pT1b-pT2b) – characteristic of the recurrence subgroup. The cohort of primary melanomas (n=12) **(paper II)** preserved as FFPE tumor blocks underwent a sectioning and staining procedure, with a slice thickness adjusted to 6 µm using a conventional microtome for sectioning. The tissue sections were placed on glass slides and stained with hematoxylin, eosin (H&E) in **paper I and II**, and additionally with BRAF V600E (VE1) mouse primary monoclonal antibody (Clone VE1, Spring-bio, Pleasanton, CA, USA) in the BRAF detection study. The monoclonal antibody staining was performed by Leica Bond Max (Leica Biosystems, Newcastle upon Tyne, UK). Dewaxing steps included high pH 9.0, EDTA based antigen retrievel for 25 min., incubation with the BRAF V600E (VE1) antibody (1:100) for 60 min., then the polymer peroxidase or alkaline phosphatase immunodetection with either fast red chromogen or specific horseradish peroxidase (HRP) based detection with DAB chromogen for 30 min and finally hematoxylin-nuclear counterstaining (**Figure 7**). For negative controls, primary antibody was substituted with the antibody diluent buffer containing 1% goat normal serum. Following staining, immunoreactions were scanned in an automated Pannoramic slide scanner (3D Histech Ltd., Budapest, Hungary) in the BRAF detection, predictive **(paper I)**, and prognostic **(paper II)** biomarker studies.

For BRAF detection study, histopathologists, blinded to the PCR results, evaluated the stained slides. The immunostained slides were labeled as follows: diffuse positive (**Figure 7 D, E**), diffuse positive with intratumoral heterogeneity (**Figure 7, C**), focal (> 5%) positive protein expression (**Figure 7, B**), and diffuse negative or very weak staining, when there was no mutated protein expression (**Figure 7, A**).
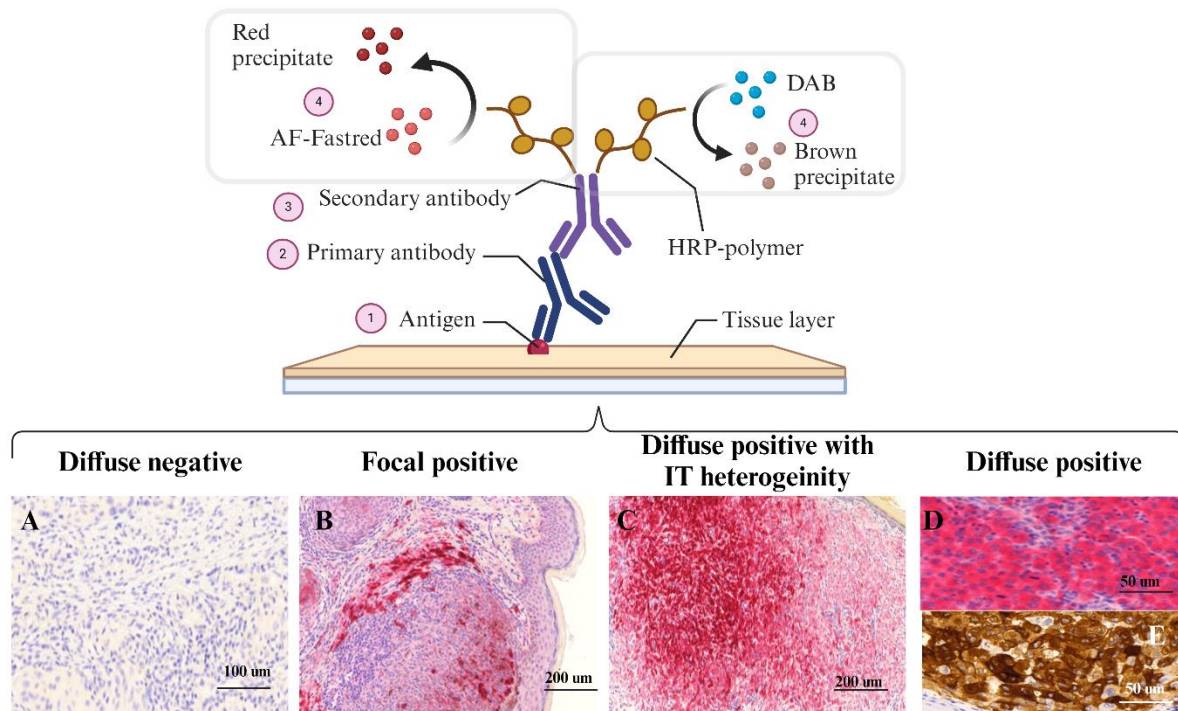

Figure 7 captures the different BRAF immunohistochemistry staining patterns with different scores using VE1 antibody clone. The upmost panel shows the mechanisms behind the IHC reaction staining including primary antibody-antigen binding (**1-2**), secondary antibody binding (**2-3**), the appearance of enzyme-based color reaction (**4**). It represents the four different staining patterns. (Either using alkaline phosphatase detection with Fastred (**A, B, C, D**) or HRP-based DAB (brown)staining (**E**). (OM 112x, scale bar from 50 μm to 200 μm)

The immunohistochemistry staining and analysis were conducted in the Department of Dermatology and Allergology in the University of Szeged.

3.5. Digital pathology and laser capture microdissection in paper II

For digital pathology and integrative image analysis, we utilized Biological Image Analysis software (BIAS, v. 1.1.1, Single-Cell Technologies)[70,71] to process a two-dimensional image file. The images were segmented using deep learning (DL) models, and a supervised machine learning algorithm (multilayer perceptron, MLP) was trained on H&E-stained FFPE tissue scans for annotating and differentiating tumor and stromal content in investigated primary melanomas (**Figure 8, A-C**). The steps of the integrative image analysis by BIAS encompassed

image pre-processing, deep-learning-based image segmentation, feature extraction, and machine-learning approaches for tissue part categorization. For segmentation the superpixels method was utilized with SLICO algorithm, and features were extracted from the segmented cells with a region size of 40 pixels, ellipse orientation, Haralick texture, and intensity adjustment. The multilayer perceptron method (MLP), a supervised learning approach with artificial neural network (ANN), was used for ML-based classification, employing backpropagation for training and K-fold cross-validation for accuracy assessment[70,71]. A detailed description of all the steps of digital pathology including the annotation method and accuracy assessment using deep-learning (DL) and machine learning method (ML) is in the publication by Szadai L. *et al*. [66].

The BIAS software interfaces with a laser microdissection microscope, making it a valuable tool for automating the isolation and collection of tumor-specific areas. The annotated H&E-stained tissue sections from 12 patient samples were prepared for automated laser capture microdissection to isolate tumor cells and surrounding stromal regions using a Zeiss PALM MicroBeam system with laser catapult (Zeiss, Germany) (**Figure 8, D**). The system, equipped with wide-field optics with a 10x objective lens ensured high cutting precision and control over contour collection, allowing for a laser cut energy range of 70- 74 and PALMRobo version 4.6 software (P.A.L.M. Microlaser Technologies GmbH, Bernried, Germany). Approximately 10,000 cells per sample (i.e., tumor: 11083 ± 5241 cells, stroma: 10152 ± 5508 cells) were collected for subsequent proteome analysis, taking into account the total area collected and the slide thickness.
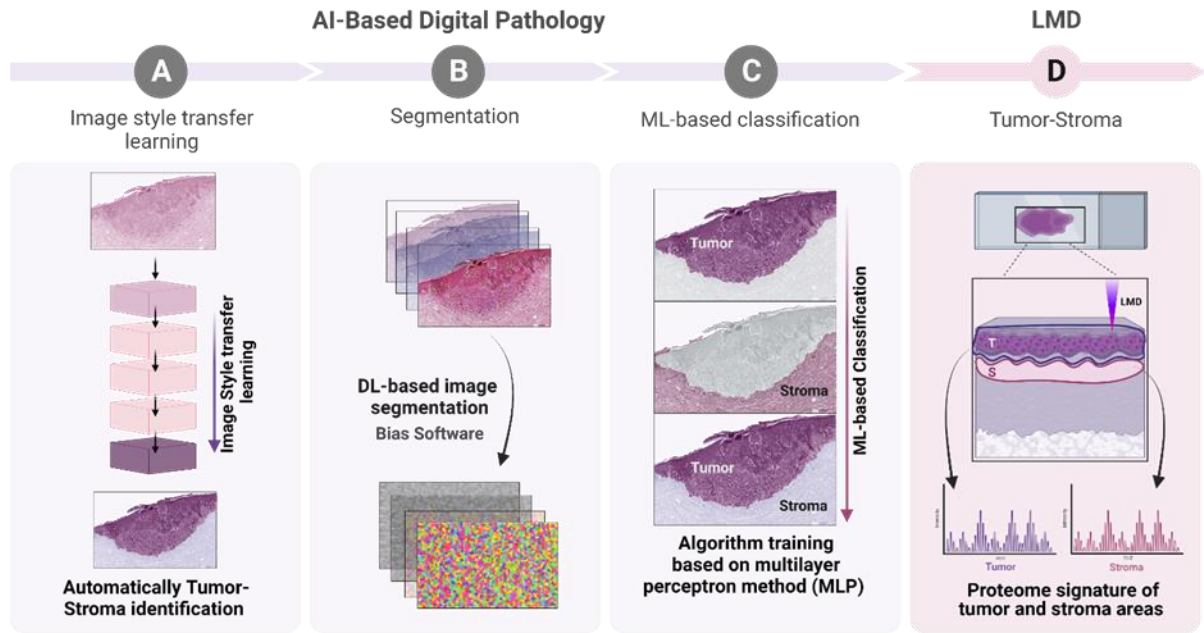
Figure 8 shows the steps of digital pathology analysis and laser capture microdissection (LMD). (**A-C**) Integrative image analysis performed by BIAS software using deep learning (DP) and machine learning (ML) approaches to automatically identify tumor and stroma areas. (**A**) Image style transfer learning was applied to FFPE tissue images to distinguish tumor and stroma areas. (**B**) Segmentation of FFPE tissue images based on DP analysis. (**C**) Algorithm training utilizing ML analysis. (**D**) Laser capture microdissection (LMD) and proteome analysis of tumor (T) and stroma (S) regions from primary melanomas with or without recurrence[66].

3.6. Proteomic analysis covering sample preparation, mass-spectrometry-based analysis, data analysis in paper I and II

In **paper I**, the sample preparation including deparaffinization, protein extraction, protein digestion, LC/MS-MS (liquid chromatography with tandem mass spectrometry) analysis and database searching were conducted based on the protocols of Velasquez, E. *et al*. (2021)[61] and Kuras, M *et al.* (2021)[72]. In the mass spectrometer settings, all the proteomic analysis was used in a data-dependent acquisition mode (DDA). The proteomic data was searched against the UniProt human database (as of May 26, 2020) and two spectral libraries were utilized, including the Proteome tools HCD 28 PD and NIST Human Orbitrap HCD, using the Proteome Discoverer 2.4 software from Thermo Scientific. To correct for batch effect, a continuous batch correction method implemented in the proBatch R package (v. 1.6.0)[73] was utilized. Mass spectrometry analysis detected and quantified 7881 protein groups across all datasets. In **paper II**, microdissected tissue samples were processed for proteomic analysis based on the protocol of Velasquez, E. *et al.* (2021)[61] and Pirhonen, J. *et al*. (2022)[65], employing a variable window data-independent acquisition (DIA) method for mass spectrometry (MS)

data acquisition. The DIA-NN (neural network) software was conducted to perform a protein database search on the DIA runs in direct mode, utilizing the human reference database from the UniProt repository (2022). Protein identification and quantification were conducted using a label-free approach with an FDR (false discovery rate) of 1%, resulting in detection of 7484 proteins. The data underwent processing using the Perseus platform[74] and the abundance values were log2 transformed and then subtracted by the median of all identified proteins in the sample as well as in **paper I.** For partial least squares-discriminant analysis (PLS-DA), 5401 proteins, corresponding to 70% of valid values in the entire cohort, were utilized, and imputation was performed on the remaining missing data in **paper II**. The detailed description of all steps of proteomic analysis of **paper I** and **II** can be found in the publication by Szadai L. *et al*. [64,66].

3.7. Code availability

For **paper I**, the scripts used for proteomic data normalization, batch effect correction and statistics are available at https://github.com/bszeitz/MM_pilot (accessed on 10 July, 2024). The summary of the statistical analyses on proteomic data including Cox regression analysis results for immunotherapy subgroup provided in Supplementary Document S1 of **paper I**. For **paper I**, proteomic data generated in the study were deposited in PRIDE consortium. Project accession is PXD028930, username is reviewer_pxd028930@ebi.ac.uk, and password is TaHGkBGm.

3.8. Statistical analysis

In the BRAF detection study, non-parametric statistical analysis (Pearson Chi^2 test with cross tabulation) was performed using IBM SPSS statistics software version 27 (SPSS Inc., Chicago, IL, USA)[75] to compare the results of PCR, IHC, and staining markers. P value less than 0.05 was considered statistically significant.

After the database searching, all proteomic data post-processing steps and subsequent statistical tests in **paper I** were performed in R v. 4.0.4 using RStudio v. 1.4.1106 (RStudio, Boston Massachusetts, USA)[76]. Visualizations were made using ggplot2 v.3.3.3[77], ggbiplot v.0.55[78], cowplot v.1.1.1[79], gridExtra v.2.3[80] and ComplexHeatmap v.2.6.2[81]. Survival analysis identified potential predictors of long or short progression-free survival after the patients received immunotherapy using Cox regression models (alpha was set to 0.05 and nominal p-values less than 0.05 were considered as significant), and protein networks were constructed using STRING (v.11.5)[82]. Samples were then stratified based on tumor type (Primary or Metastasis). Cytoscape (v.3.8.2)[83] was performed for overrepresentation analysis of GO

biological processes[84] and KEGG pathways [85]. The processes with FDR values below 0.05 were visualized and interpreted for biological significance.

In **paper II**, significantly dysregulated proteins were identified if the FDR was 5%, employing the Two-stage step-up (Benjamini, Krieger, and Yekutieli) method incorporated in the software. Graph Pad Prism 9 (Graph Pad Prism Software Inc. version 9.0.0, San Diego, California, USA)[86] was also used for determining the dysregulated proteins between the groups. Gene Set Enrichment Analysis (GSEA)[87] was carried out on the complete dataset after normalization and standardization, utilizing HALLMARK[88] and REACTOME[89] Version 2022 gene set databases in the analysis in **Figure 12**. Throughout the thesis, **Figure 1-8** and **Figure 10-12** were created with Bio Render 2021 software (Bio Render, Toronto, ON, Canada)[90]. **Figure 9** was created using Graph Pad Prism 9 (Graph Pad Prism Software Inc. version 9.0.0, San Diego, California, USA)[86]. **Table 1-4** were created with Microsoft Excel. (Microsoft 365, Microsoft Corporation, Redmond, Washington, USA).

3.9. Ethical approval

The three studies were conducted according to the guidelines and regulations from the Swedish biobanking laws and from the Declarations of Helsinki, and approved by the Hungarian Ministry of Human Resources, Deputy State Secretary for National Chief Medical Officer, Department of Health Administration. The protocol code is MEL-PROTEO-001, the approval number is 4463-6/2018/EÜIG and the date of approval is 12 March 2018. The approval numbers for the most recent modifications are 2852-5/2023/EÜIG (10th February, 2023) and 2852-10/2023/EÜIG (12th July, 2023).

4. Results

Based on the BRAF detection study, the predictive biomarker study **(paper I)** and the prognostic biomarker study **(paper II)**, here I summarize the results of these studies.

4.1. Results of the BRAF detection study

4.1.1. Comparison of IHC findings with PCR results

In the management of advanced melanomas, it is pivotal to select an eligible therapy with high efficiency. Therefore, the initial step should involve recognizing detailed characteristics of the melanoma, such as the BRAF mutation status, which forms the basis for targeted therapy. In this study, we aimed to compare two diagnostic methodologies, a genome

and a protein based approach, to find the most appropriate tool in BRAF mutation detection (**Figure 9**).

In this cohort, Sanger sequencing was performed on 94 samples to detect BRAF and cKIT mutations, revealing BRAFV600 mutations in 43 samples. BRAFV600E mutation was observed in 32 cases, while BRAF V600R in 2 cases, V600K in 8 samples, and K601E was identified in only one melanoma. BRAFV600E mutation expression was predominantly detected in superficial spreading and nodular melanomas, while a single acrolentiginous melanoma sample exhibited cKIT mutation. All the 94 immunohistochemistry slides from FFPE samples underwent staining using the VE1 antibody. For IHC staining, alkaline-phosphatase reaction with fast red chromogen in 66 cases, while horseradish peroxidase based detection with DAB chromogen (brown) was applied in 28 cases. The VE1 clone, is specific for BRAFV600E mutated protein, did not detect other V600 mutations. Therefore, 11 cases with BRAFV600K, R and K601 mutations were excluded both from the immunohistochemistry results and from the specificity, sensitivity values. Based on the various VE1 antibody staining patterns, we classified the samples into four groups: roughly one-third of IHC staining cases displayed diffuse negative or very weak staining for the BRAF V600E mutated protein. Thirty-two cases exhibited diffuse positive staining, 8 showed diffuse positive staining with intratumoral heterogeneity, and 11 displayed focal positive staining (**Figure 9**).
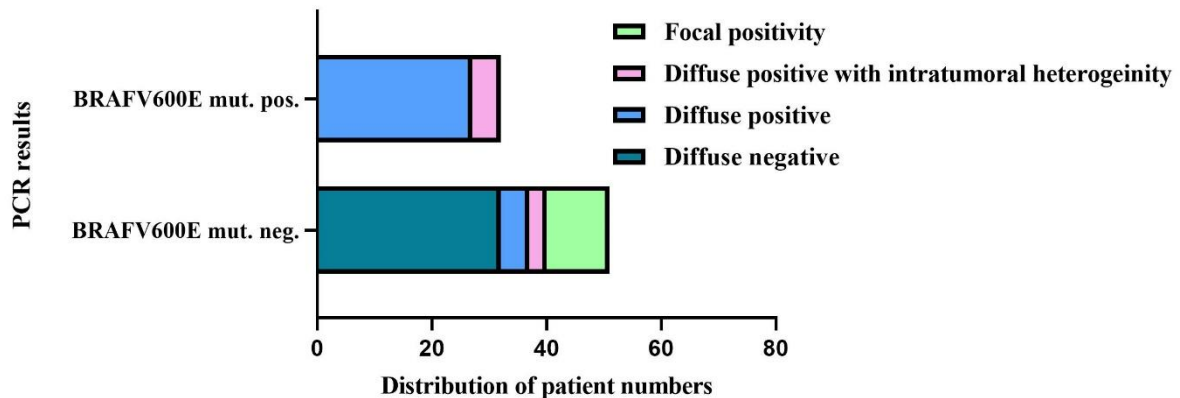
PCR	IHC				
	Diffuse neg. (*N*)	Diffuse pos. (*N*)	Diffuse pos. IT het. (*N*)	Focal pos. (*N*)	All
V600E mutation pos. (*N*)	0	27	5	0	32
V600E mutation neg. (*N*)	32	5	3	11	51
All	32	32	8	11	83

Figure 9 represents the comparison of the results of BRAFV600E mutation using PCR and the intensity of BRAFV600E VE1 antibody via immunohistochemistry (IHC) staining in a box-plot (above) and summarizes the

data in a table (below). Other V600 mutations were disregarded from the comparison. /pos. –positive, neg.- negative, IT het. – intratumoral heterogeneity, N – number/

A comparison between PCR and IHC methods revealed significant discordance (Pearson Chi^2 test, p <0.05). It means that among the PCR-negative cases, IHC revealed five cases with diffuse positivity, three samples with diffuse positivity and intratumoral heterogeneity, and 11 samples with focal positivity staining patterns (see **Figure 9**). In terms of IHC sensitivity, all melanoma cases diagnosed positive for BRAF V600E via PCR demonstrated varying degrees of positive IHC results. Notably, none of the PCR-positive cases exhibited focal positive IHC expression. In our comparative analysis, BRAFV600E detection via IHC demonstrated 100% sensitivity alongside 63% specificity, with positive and negative predictive values of 63% and 100%, respectively. Sensitivity indicated the percentage of cases in which PCR-detected BRAF mutations were correctly identified by IHC. Specificity indicated the percentage of cases where PCR negative mutation results were accurately not identified by IHC as BRAF-positive staining.

4.1.2. Results of molecular analysis of BRAF positive cases validated by IHC

Immunohistochemistry revealed focal expression of the V600E mutated protein in 11 samples, in which the PCR sequencing did not detect any mutations in these melanoma samples. In our validation study, nine cases out of the aforementioned 11 samples underwent next generation sequencing (NGS) analysis to explore potential mutations in the BRAF contributing to the focal expression pattern. Prior to the analysis, tumor and stroma were distinguished and marked, and the entire tumor section was examined, including the focal positive areas. Only one sample out of nine revealed the BRAF D594N aberration (rs397516896; c.1780G>A), with a variant frequency of 1.90%. In the remaining eight cases, the NGS did not demonstrate any BRAF mutations in the region of interest (see **Table 4** and **Materials and Methods**).

IHC	PCR with Sanger seq.	NGS	qPCR
focal positive	WT (neg.)	c.1780G>A; D594N	-
focal positive	WT (neg.)	WT (neg.)	-
focal positive	WT (neg.)	WT (neg.)	-
focal positive	WT (neg.)	WT (neg.)	-
focal positive	WT (neg.)	WT (neg.)	-
focal positive	WT (neg.)	WT (neg.)	-
focal positive	WT (neg.)	WT (neg.)	-
focal positive	WT (neg.)	WT (neg.)	-
focal positive	WT (neg.)	WT (neg.)	-
diffuse pos. with IT	WT (neg.)	-	below LOD, WT
diffuse pos. with IT	WT (neg.)	-	WT
diffuse pos.	WT (neg.)	-	WT
diffuse pos.	WT (neg.)	-	WT
diffuse pos.	WT (neg.)	-	MUT
diffuse pos with IT	WT (neg.)	-	below LOD, WT
diffuse pos.	WT (neg.)	-	below LOD, WT
diffuse pos.	WT (neg.)	-	WT

Table 4 provides a detailed comparison of the results of IHC staining, PCR, NGS, and qPCR. For NGS, one mutation was identified, similar to qPCR. In qPCR, three cases were below the threshold range. / Sanger seq. – Sanger sequencing, WT- wild type, IT – intratumoral, pos. – positive, neg. – negative, LOD - limit of detection/

In accordance with immunostaining, we observed diffuse positivity in five cases and diffuse positivity with intratumoral heterogeinity in three cases, wherein PCR did not detect any mutations at DNA level. Therefore, to investigate this discrepancy, we conducted real-time polymerase chain reaction (qPCR). Among the eight cases, only one harbored the BRAFV600E mutation, while three cases remain within the borderline range (**Table 4**). These samples were confirmed as negative based on the protocol outlined in the **Materials and Methods** section.

4.2. Results of the predictive biomarker study (paper I)

4.2.1. Proteomic analysis unveils proteins and pathways indicating survival outcome in the immunotherapy treated patient group

In the predictive biomarker study (**paper I**), we have conducted an extensive proteomic analysis on 90 FFPE melanoma samples from 77 mainly advanced melanoma patients. This analysis aimed to represent the potential molecular changes between samples, and identify proteins predictive of immunotherapy response (**Figure 10**).

Our study aimed to answer the following question: Can proteomics unveil new potential biomarkers or dysregulated pathways predictive of therapy response? A total of 90 samples from 77 patients underwent analysis based on their clinical and global proteomic expression data. Mass spectrometry analysis quantified 7881 protein groups across all datasets[64]. Patients were categorized based on their primary treatment, including immunotherapy. The immunotherapy patient group comprised 24 samples from 22 patients. These samples were

treatment-naive, allowing observation of their protein expression profiles prior to therapy initiation. To identify potential predictors, multiple Cox regression models were constructed using progression-free survival (PFS), protein expression data, stratified by sample type, i.e., primary or metastasis. The analysis revealed 401 proteins significantly correlated with survival in the immunotherapy patient group (Multiple Cox regression p-value < 0.05). These significant proteins were visualized in heatmap (**Figure 10, A**).
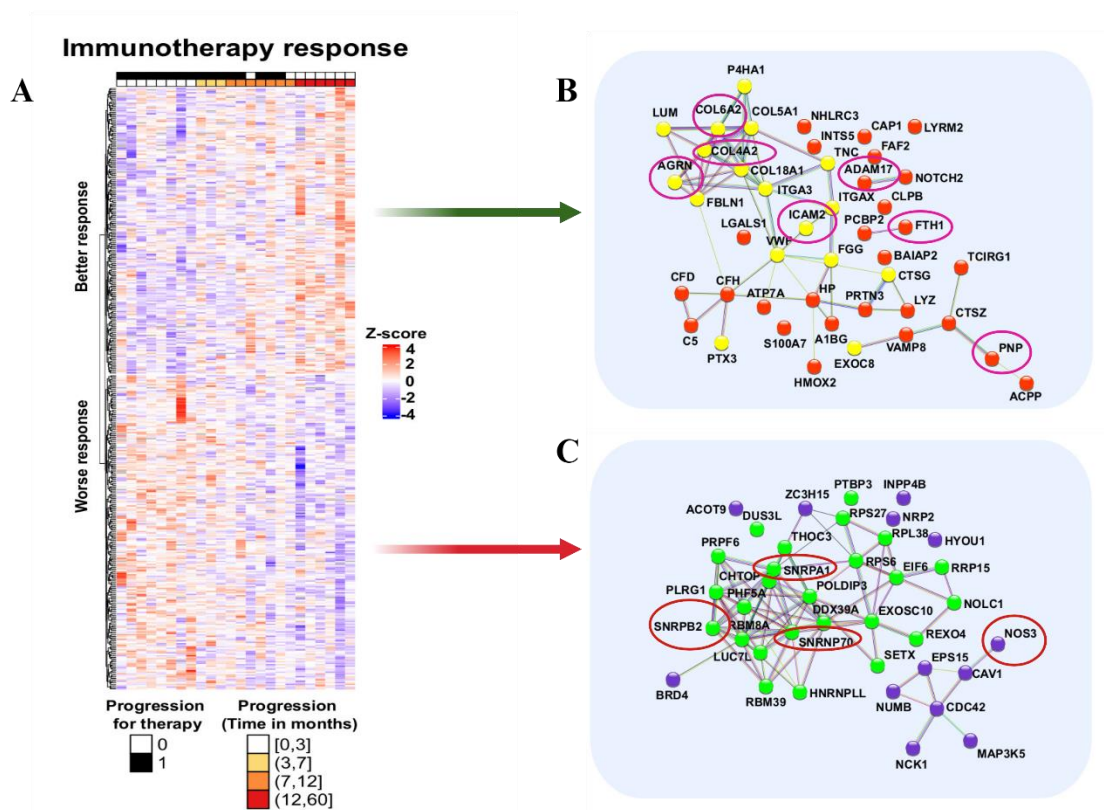
Figure 10 displays the heatmap and the network of protein–protein interactions of the up- and downregulated proteins in patients received immunotherapy. (**A**) Heatmap illustrates the expression patterns of pathways and proteins in the therapy response subgroups (blue color indicates downregulation in protein expression, red color represents upregulation in protein expression). (**B**) presents the network of protein-protein interactions in patients with favorable therapy response (the yellow color represents the extracellular matrix components, while the red color signifies the components from the immune system, pink circle shows the highlighted proteins mentioned in the text) (**C**) displays the network of protein-protein interactions in patients with worse immunotherapy outcome (proteins involved in RNA processing are highlighted in green, while members of the VEGFA-VEGFR2 pathway are shown in purple)[64].

The functional analysis of proteins (Gene Ontology (GO) terms, KEGG pathways, Reactome, Wikipathways) revealed distinct activated pathways for patients with different progression-free survival (PFS) durations. In the subgroup with shorter PFS after immunotherapy, significantly upregulated proteins were associated with cellular and metabolic processes, including the VEGFA-VEGFR2 pathway (**Figure 10, C**) (KEGG pathway database: FDR < 0.05). Additionally, in connection with the VEGFA-VEGFR2 pathway, downregulation of the nitric oxide synthase 3 (NOS3) expression was observed in patients with longer PFS following immunotherapy treatment (Cox regression test p < 0.05) (**Figure 10, C**).

Similarly, upregulation of proteins involved in RNA splicing mechanisms was detected in patients receiving immunotherapy who exhibited a lack of tumor response (i.e., started to progress after a few months). Notably, proteins from the splicing processes such as SNRPB2, SNRNP70, and SNRPA1 were significantly upregulated (GO Biological Process, FDR < 0.05) (**Figure 10, C**) in this immunotherapy subgroup.

We also discovered proteins that are potential predictors of improved response to immunotherapy (**Figure 10, B**). Within this protein subgroup, signatures induced by stroma and components of the immune system were notably overrepresented. Among the proteins and pathways significantly upregulated (KEGG pathways, GO biological processes, FDR < 0.05) in the subgroup with a better response to immunotherapy were those involved in functions such as complement cascade, B-cell differentiation, neutrophil degranulation (e.g., PNP (Purine nucleoside phosphorylase), Ferritin heavy chain 1 (FTH1)), immunoregulation (e.g., ADAM metallopeptidase domain 17 (ADAM17)), ECM-receptor interaction (e.g., AGRN (Agrin) protein), integrin cell surface interactions and cell adhesion (e.g., ICAM2 protein, COL4A2 and COL6A2 proteins) (KEGG pathways, GO biological processes, FDR < 0.05) (**Figure 10, B**).

4.3. Results of the prognostic biomarker study (paper II)

4.3.1. The clinicopathologic features of the utilized melanoma samples

In this study, we performed an in-depth analysis of 12 early-stage primary melanoma samples (AJCC8 IA-IIA at diagnosis) to investigate molecular and histopathological markers associated with disease recurrence within a 5-year period after diagnosis. The samples were divided into two groups: those with recurrence (n = 6) and those without recurrence (n = 6). Our histopathological assessment revealed a clear correlation between tumor thickness (Breslow and Clark levels) and recurrence. Additionally, tumors from both groups represented various features characterized by SSM with distinct cellular proliferation, vascular

development, and immune cell infiltration. However, these parameters alone were not conclusive markers of high recurrence risk. Our analysis of clinical data indicated that Breslow level (Mann–Whitney U test: $p = 0.0022$) and clinical stages (IA–IIA) (Fisher exact test: $p = 0.0606$) influenced recurrence.

4.3.2. From digital pathology to laser capture microdissection

Artificial intelligence-based digital pathology (AI-DP) is redefining the idea of general clinical pathology by enhancing quantitative accuracy and facilitating data categorization through spatial algorithms. In this study, H&E-stained scanning images were employed to train AI-based digital pathology (AI-DP) with the BIAS v.1.1.1 (Single-Cell Technologies), integrating deep learning and machine learning algorithms, to enhance the accuracy of identifying tumor and stroma cells in early-stage primary melanomas from histological images. In this study, ten distinct images were utilized for training and optimizing the pipeline. Reparameterization was applied during the training process to improve detection accuracy. The implemented workflow successfully recognized tumor and stroma regions, along with normal epidermis, dermis, glands, and connective tissues (**Figure 11**). The algorithmic pipeline was trained to achieve an overall segmentation accuracy of approximately 80% (Recurrence: $81.7 \pm 6.3\%$, no recurrence $78.0 \pm 3.6\%$), corroborated by certified pathologists. Importantly, this AI-driven methodology demonstrated equal effectiveness in distinguishing normal tissue from stromal and tumor regions across both recurrent and non-recurrent primary melanomas (**Figure 11**). Subsequently, these samples were subjected to laser microdissection for the isolation of tumor and stroma components, which were subsequently prepared for quantitative proteomics.
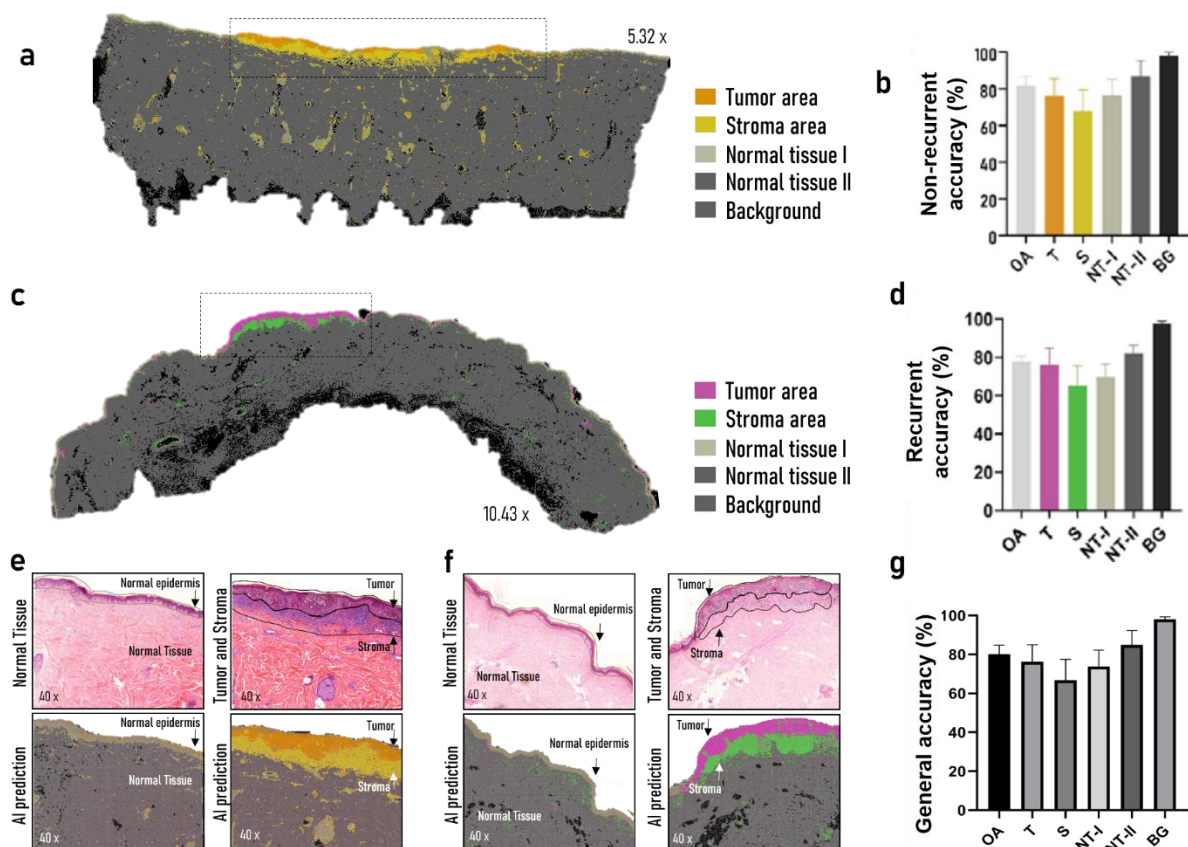
Figure 11 displays a representative tumor-stroma prediction using the AI-DP approach for non-recurrent and recurrent melanomas. **A**) AI-prediction of tumor (Dark yellow) and stroma (Light yellow) areas in a non-recurrent primary melanoma tissue. **B**) AI accuracy (%) prediction for non-recurrent melanoma samples. **C**) AI-prediction of tumor (Dark pink) and stroma (Light green) areas in a recurrent primary melanoma tissue. **D**) AI accuracy (%) prediction for recurrent melanoma samples. **E**) Comparison between manual annotation of normal tissue areas and tumor-stroma areas with hematoxylin-eosin staining and AI-prediction in a non-recurrent melanoma. **F**) Comparison between manual annotation of normal tissue area and tumor-stroma area with hematoxylin-eosin straining and AI-prediction in a recurrent melanoma. **G**) General AI accuracy (%) prediction for the entire cohort. Error bars represent relative standard deviation (RSD %) among the samples present in the group.[66] /Data: OA-Overall, T-Tumor, S-Stroma, NT-I Normal tissue I (normal epidermis and glands), NT-II Normal tissue II (dermis and connective tissue), BG-Tissue background. /

4.3.3. Distinct proteomic signatures in tumor and in stroma among different recurrence status groups

A comprehensive proteome profiling was achieved utilizing HR-DIA-MS (high resolution data-independent acquisition mass spectrometry) with identifying over 7000 proteins across all samples. Hierarchical clustering and PLS-DA analysis unveiled clear proteomic differences between tumor and stromal compartments across different recurrence status groups (**Figure 12**). While there was some overlap in the ellipses representing 95% confidence intervals regarding recurrence status, the proteomic analysis of stromal components showed

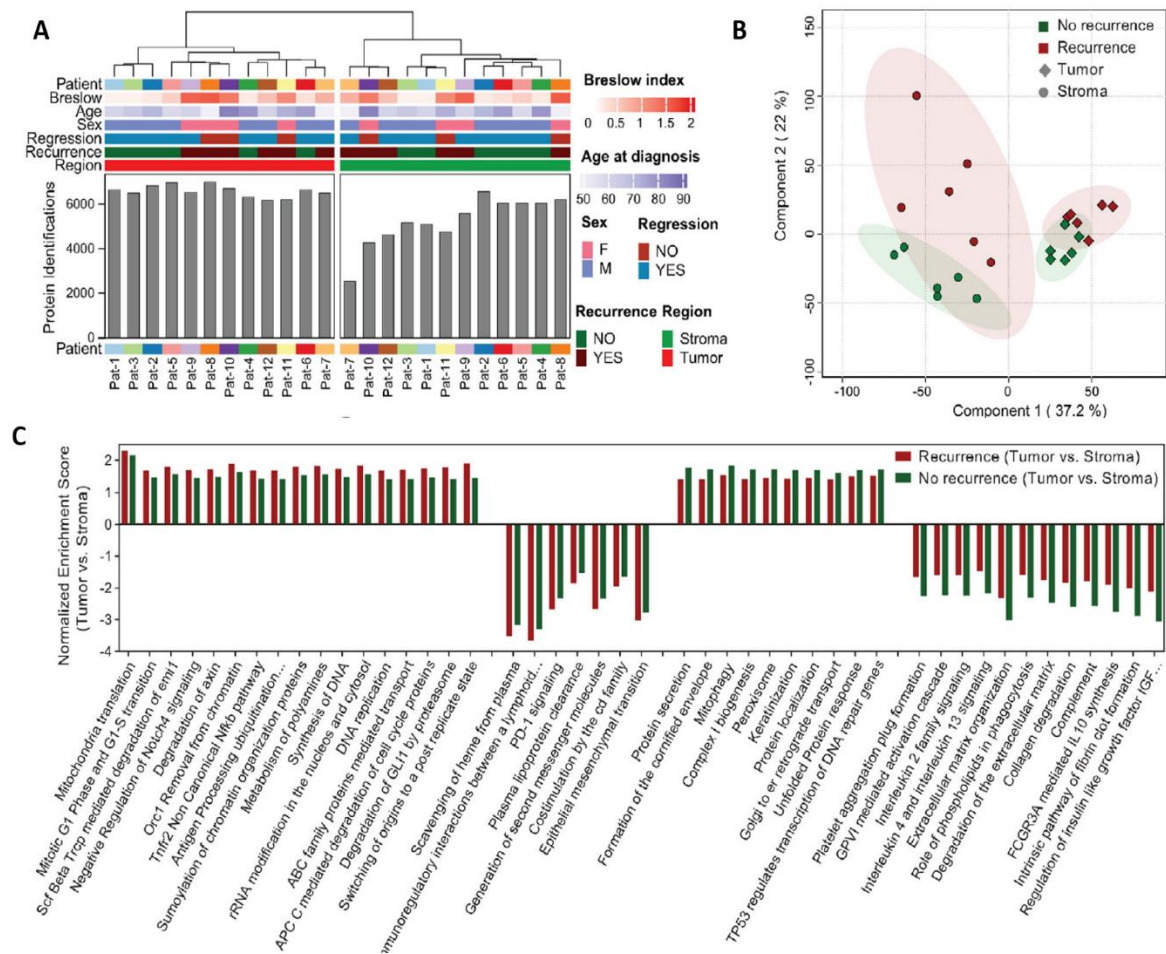better differentiation between recurrence status groups compared to tumor regions (**Figure 12, B**).

Figure 12 represents proteome profiling of tumor cells and stromal regions from recurrent and non-recurrent primary melanomas. **A)** Samples are hierarchically clustered based on their proteomic abundance profiles. The bar chart illustrates the number of proteins identified in each sample. **B)** PLS-DA utilizes proteomic data from the sample cohort. Proteins included had a minimum of 70% valid values across the entire cohort, the remaining missing data were imputed. **C)** Gene Set Enrichment Analysis (GSEA) comparing tumor and stromal regions in the recurrent and non-recurrent groups. The bar chart represents the normalized enrichment score for the most divergent significantly dysregulated functional annotations between recurrent and non-recurrent groups. Positive scores indicate upregulated while negative scores indicate downregulated in tumor cells compared to the microenvironment. The analysis on recurrent primary melanomas is represented by red bars while green bars correspond to the analysis on non-recurrent melanomas. [66]. /F-female, M-male, No. – number, NES – normalized enrichment score/

Building upon the initial unsupervised analysis, we stratified the sample cohort into four categories based on sample origin and patient recurrence status: tumor/recurrence, tumor/no recurrence, stroma/recurrence, and stroma/no recurrence. As expected, ANOVA revealed that the comparisons between tumor and stromal components accounted for the majority of

significant differences. Between tumor and stroma samples, 2021 and 1773 proteins were significantly dysregulated in the no recurrence and recurrence groups, respectively. Among the recurrence status groups, we detected 166 dysregulated proteins in tumor samples and 261 dysregulated proteins in stromal samples (FDR, q-value < 0.05). To delve into the functional molecular signature that could potentially contribute to melanoma recurrence and progression, we analyzed both the dysregulated proteins and the entire proteome. Proteomic disparities between recurrent and non-recurrent melanoma cells were examined using Gene Set Enrichment Analysis (GSEA). Results indicated a strong link between melanoma recurrence and mitochondrial activity. Recurrent melanoma tumor cells showed increased expression of mitochondrial translation machinery and key metabolic pathways like oxidative phosphorylation (OXPHOS) and the TCA cycle, crucial for mitochondrial homeostasis (FDR, q-value < 0.05). From these pathways, the level of the mitochondrial ADP (adenosine diphosphate)/ATP (adenosine triphosphate) translocases (ANT1, ANT2, ANT3), adhesion molecule (MCAM, also known as CD146) and the heterogeneous nuclear ribonucleoprotein A1 (HNRNPA1) was significantly higher in melanoma cells from the recurrence group (FDR, q-value < 0.05). These cells also exhibited heightened activity in pathways associated with cellular proliferation, protein synthesis, DNA repair, and replication (FDR, q-value < 0.05). Additionally, the downregulated proteins in recurrent melanoma cells were primarily involved in extracellular matrix organization, collagen formation, and immune responses, including the complement and coagulation cascades (FDR, q-value < 0.05).

In contrast, non-recurrent melanoma tumor cells demonstrated enrichment in pathways linked to immune response and extracellular matrix, including extracellular matrix organization, collagen formation, coagulation, complement cascade and mitophagy representing initial immune system responses (FDR, q-value < 0.05). Additionally, pathways associated with adaptive immunity, including cytokine signaling, B and T-cell receptor signaling, and antigen presentation, were also upregulated in this group (FDR, q-value < 0.05). Stromal components of recurrent primary melanomas exhibited enrichment in pathways like epithelial-mesenchymal transition and PD-1 signaling, and showed significant downregulation of immune response pathways, including extracellular matrix organization and immune cell receptor signaling compared to the stromal component in the non-recurrent group (FDR, q-value < 0.05). Conversely, the microenvironment in non-recurrent melanomas displayed more abundant features such as interleukin-related signaling pathways, collagen degradation, and complement mechanisms, compared to recurrent cases (FDR, q-value < 0.05). Moreover, intriguingly, we

found significant enrichment in mitochondrial translational in both tumor cells and stromal cells of recurrent melanomas compared to non-recurrent melanomas (FDR, q-value < 0.05).

4.4. Limitations

Acknowledging the limitations of our metastatic cohort in the predictive biomarker study (**paper I**), such as sample heterogeneity due to different histology types and clinical parameters, we note that tumor content varied from a few percent to 90%, potentially impacting therapy response mechanisms related to stromal cells. The upregulation of EC components in some samples suggests the influence of tumor content differences on proteomic profiles. Regarding the BRAF detection study, in the case of validation of focal positive cases via next-generation sequencing, due to technical difficulties, only 9 out of 11 cases were analyzed by next-generation sequencing. Concerning the prognostic biomarker study (**paper II**), the restricted sample size of the study emphasizes its limitations. Furthermore, the samples used for validation were also employed in training the digital pathology with AI driven imaging algorithms.

5. Discussion

In this thesis, three main studies were summarized focusing on identifying biomarkers with prognostic and predictive approaches via IHC, quantitative proteomics and digital pathology with AI-driven imaging.

Regarding the predictive targets of melanoma in routine diagnostics, the detection of BRAF mutation is a crucial step in selecting appropriate therapies for advanced melanoma patients. Therefore, the timing and the adequate method for the BRAF mutation is essential. New initiatives are underway for BRAF mutation detection in melanoma care. While DNA-based PCR is the gold standard, immunohistochemistry staining is increasingly recognized for its practicality and cost-effectiveness[28–30].The BRAF detection study presented the comparison of DNA-based PCR and the protein-based IHC diagnostic methodologies for detecting BRAF mutations in melanoma. The IHC staining of BRAFV600E on FFPE slides provides valuable and additional information about the characteristics of the tumor and protein expression patterns. For instance, multiple studies have emphasized the importance of strong, diffuse staining of the VE1 clone, suggesting its utility as an indicator of BRAF-positive melanomas for targeted therapy selection[29]. In tumor histopathology, it's also vital to recognize intratumoral and intertumoral heterogeneity, as evident in our IHC categorization (diffuse negative, diffuse

positive, diffuse positive with intratumoral heterogeinity and focal positive cases)[91–95]. For instance, primary and metastatic tumors may exhibit different BRAF mutation patterns due to intertumoral heterogeneity[91]. Therefore, multiple diagnostic methods are needed, as relying on a biopsy with a false-negative BRAF status might exclude patients who could have therapy response to targeted treatments[91]. Furthermore, the various staining patterns pointed out the fact that in cases of predominantly BRAFV600E melanoma, it's essential to also consider the presence of wild-type BRAF minor subclones, as these mutations could contribute to therapy resistance[96].

We demonstrated that despite the high sensitivity of IHC in detecting BRAF V600E mutated proteins, it showed that even automated immunohistochemistry may suffers limitations in specificity, potentially due to false positive results. According to the literature, these results could come from different BRAF point mutations or antibody cross-reactions[28]. Therefore, these significant mismatched results (Pearson Chi^2 test, $p < 0.05$) were further validated by NGS and qPCR techniques in our study. Further detailed qPCR sequencing revealed one case of BRAFV600E positivity initially diagnosed as PCR negative. This case was identified among the diffuse positive cases showing varying degrees of intratumoral heterogeneity detected by IHC. This result suggests a potential dilution artifact in the mutated DNA, highlighting a limitation of the PCR method. Next-generation sequencing analysis was conducted on the focal positive cases. Remarkably, the thorough DNA sequencing revealed a genetic-level mutation, specifically the BRAF D594N aberration, only in one sample. NGS conducted on FFPE slides may lead to DNA degradation due to formalin fixation, potentially causing false NGS results. Variant allele frequencies >1.5% in hotspot regions are deemed acceptable if reproducible. A minimum of 200 cells is required for NGS analysis to detect 1.5% mutant DNA copies, considering possible allele dropout. The detection of BRAF mutation in one case by a precise method (NGS)[97], highlights the need for detailed DNA-based PCR analysis in equivocal or focal BRAF IHC staining cases. The results from both NGS and qPCR emphasize the importance of employing diverse methods to detect BRAF mutations. This underscores the idea that depending solely on one technique for analyzing a tumor with high mutation rate might not be ideal, and promotes the combined usage of the PCR and IHC techniques.

Moving forward to proteomics, we were able to detect biomarkers with prognostic and predictive values from archived formalin-fixed paraffin-embedded melanoma samples. In the predictive biomarker study (**paper I**), through proteomic analysis, distinct molecular signatures associated with immunotherapy response were uncovered. Regarding the immunotherapy

subgroup with worse response, proteins of the VEGFA-VEGFR2 pathway were upregulated. Activation of the VEGFA-VEGFR2 pathway is linked to endothelial cell growth, vasculogenesis, and metastatic potential of the tumor, suggesting a prognostic signature for locoregional lymphatic metastasis[98]. In a study that did not explore immunotherapy connections, it was demonstrated that while PD-1 expression correlates with higher survival rates, VEGFA expression is associated with a worse prognosis in lymph node metastasis[99]. Recently, VEGFA blockers have been utilized in anticancer therapies, such as in the case of lung cancer[100] treatment, or anti-angiogenic drugs like humanized anti-VEGF monoclonal antibody, bevacizumab (Avastin), which is a first-line treatment in metastatic colorectal cancer, and has already been approved by the FDA[101]. These findings support the potential role of VEGFA blockers in melanoma treatment. Noteworthy, NOS3, in connection to the VEGFA-VEGFR2 pathway, showed downregulation in patients with longer progression-free survival in the immunotherapy subgroup, and it is known that the production of NOS3 (NO) promotes VEGF-induced angiogenesis[102], tumor progression, and proliferation[103]. Furthermore, proteins in pathways of RNA splicing also showed an upregulation pattern in the immunotherapy subgroup with worse response. It is confirmed that abnormal splicing mechanisms have been associated with tumor progression[104]. These disordered splicing mechanisms could lead to the loss of cell surface antigens, which are pivotal in melanoma and immune cell interplay, potentially contributing to immunotherapy resistance[104]. Several studies have explored small molecules that hinder splicing mechanisms, yet the efficacy and safety of these methods remain under investigation[105,106]. Nonetheless, the identification of anti-spliceosome drugs may offer potential therapeutic strategies to overcome immunotherapy resistance. In the immunotherapy subgroup with better response, proteins from the ECM and the immune system were significantly upregulated. From the immune system, specifically neutrophil degranulation pathways showed an overexpression pattern. This result was consistent with the literature since an in-depth plasma proteomics study by Babačić et al. indicated that increased neutrophil degranulation with elevated neutrophil-to-lymphocyte ratio, observed during anti-PD-1L therapy, was associated with longer overall survival[107]. Moreover, proteins connected to neutrophil degranulation (PNP, FTH1) and immunoregulation (ADAM17) showed upregulation in this patient subgroup with potential to treatment targets. For instance, purine nucleoside phosphorylase (PNP) catalyzes the reversible phosphorolysis of purine nucleosides[108], and however contrary to our findings, but some studies suggest that PNP inhibitors as a promising agent could contribute to melanoma treatment[109,110]. Additionally, ferritin heavy chain 1 (FTH1) is a crucial protein for iron homeostasis[111]. It has been

demonstrated that FTH1 levels are significantly associated with the infiltration of tumor-associated macrophages and play a pivotal role in regulating tumor immunity in solid cancers[112], potentially affecting immunosuppression in melanoma[113]. Furthermore, ADAM metallopeptidase domain 17 (ADAM17), is involved in shedding certain cell membrane proteins and regulating various signaling pathways, particularly in immunoregulation[114]. For instance, it is known that the ADAM-mediated shedding of LAG3 from the cell surface is crucial for effective anti-tumor immune mechanisms[115]. It was also published that there was a positive association with tumorigenic CD163 macrophages and expressed ADAM17 level[114]. It was also reported that the ADAM17/EGFR/AKT/GSK3β axis plays an important role in regulating melanoma cell migration, proliferation, and sensitivity to chemotherapeutic drugs[114,116], providing new insights into the role of ADAM17 in melanoma treatment.

Besides the immune response, the function of extracellular organization in the tumor microenvironment is noteworthy. Various studies have underscored the interplay between ECM proteins and the immune system in melanoma. For example, Fejza *et al*. found an association between ECM proteins and the efficacy of PD-1 treatments[117]. Interestingly, in our study, ECM proteins, particularly those involved in cell adhesion components (e.g., ICAM2 protein, COL4A2, COL6A2), were upregulated and correlated with longer survival rates and better responses to immunotherapy. In contrast, the ECM also serves as a foundation for the pre-metastatic niche, a potential target for anti-cancer therapies. Recent research has outlined mechanisms crucial for preventing the development of metastatic environments[118], including the targeting of EC vesicles such as CXCR2 and CXCR4 inhibitors[118]. These findings highlight proteins and pathways that can be ideal target during immunotherapy in melanoma.

For the more detailed understanding of the stroma, in the third study (**paper II**) we identified prognostic proteins with novel approaches such as digital pathology with AI-based imaging and quantitative proteomics from formalin-fixed paraffin-embedded early-stage melanoma samples. This study highlights the critical role of tumor-microenvironment interactions in primary melanoma development and recurrence[119]. Histopathological assessment revealed varied characteristics across risk categories. In line with other studies, Breslow and Clark levels were indicative for high recurrence risk[51]. Moreover, our application of AI-based digital pathology (AI-DP) utilizing BIAS software and deep learning models to analyze H&E-stained scanning images has revolutionized conventional clinical pathology by improving quantitative precision[70]. This method effectively distinguished tumor and stroma regions with an approximate accuracy of 80%, showcasing the capability for automated selection and retrieval

of tumor-relevant areas. Despite promising results, the small sample size of the study limits broader conclusions. Larger cohorts are needed, especially for AI-based digital pathology in early-stage melanomas.

From the comparison of the proteomic results of the isolated tumor and stroma, we have found critical mechanisms involved in tumor growth and progression, such as cellular translation machinery, DNA repair and replication, which were upregulated in recurrent tumor regions compared to their stromal regions. Notably, tumor cells from patients with recurrent melanomas showed a more pronounced enrichment in proliferation pathways, particularly mitochondrial translation, when contrasted with non-recurrent tumor regions, highlighting the significance of mitochondrial function in cancer progression[120]. Moreover, the overexpression of mitochondrial metabolic pathways, including oxidative phosphorylation and the TCA cycle, in tumor cells from patients with recurrent melanomas indicates a high demand for energy production, crucial for sustaining tumor cell proliferation by maintaining mitochondrial dynamics and homeostasis. Concurrently, the upregulation of specific proteins such as the mitochondrial ADP (adenosine diphosphate)/ATP (adenosine triphosphate) translocases ANT1, ANT2, and ANT3 indicates increased ATP flux to meet cellular energy demands and drive disease recurrence[121]. Additionally, MCAM (as also known as CD146) promotes angiogenesis and hematogenous metastatic spreading[122], while HNRNPA1 regulates pyruvate kinase isoforms, contributing to metabolic reprogramming in melanoma cells[123]. These proteins from the recurrence group signifies a more aggressive phenotype and an increased risk of disease recurrence. Consistent with these findings, it was also published that critical mitochondrial processes, including oxidative phosphorylation and mitochondrial translation machinery, are significantly enriched in BRAF V600E samples, driving melanoma progression[124]. Furthermore, the higher activity of pathways like epithelial-mesenchymal transition and PD-1 signaling in the stromal component of recurrent melanomas underscores the pivotal role of the tumor microenvironment in modulating the immune response and fueling tumor progression and potential recurrence[125–127]. The overexpression of PD-L1 in stromal cells, coupled with its interaction with the PD-1 receptor on adaptive immune cells, can initiate a signaling cascade that suppresses immune surveillance. This mechanism has significant therapeutic implications, such as the use of PD-L1 and PD-1 inhibitors in these early-stage melanomas. Conversely, tumor cells from non-recurrent melanomas show an abundance of immune system response-related pathways, suggesting robust immune reactions that could potentially prevent disease recurrence. These findings align with previous studies emphasizing

the importance of mitochondrial function and immune response-related pathways in melanoma progression and recurrence[120,125,128,129]. Moreover, in respect to therapeutic approaches, Gil *et al.* found that antibiotics, especially Doxycycline, Tigecycline and Azithromycin, reversibly targeting the mitochondrial 30S-50S subunits of bacteria, and interestingly they were able to show in vitro that these three drugs could inhibit the proliferation of melanoma cell lines in a dose-dependent manner[130]. Interestingly, several publications highlight the role of metformin in inhibiting the mitochondrial function[131,132]. Metformin is one of the most commonly used anti-diabetic drug, and it has been shown to reversibly inhibit mitochondrial complex I, reducing mitochondrial oxidative phosphorylation and ATP consumption[131,133–137]. By regulating the mammalian target of rapamycin complex 1 (mTORC1), it eventually inhibits the proliferation of tumor cells[131,133–136,138]. Additionally, metformin has been shown to cause the phosphorylation of programmed death ligand 1 (PD-L1), leading to its degradation and subsequently facilitating the T-lymphocyte-mediated tumor cell death[137,139,140]. It also reduces the activity of immunosuppressive cells (e.g., M2-like tumor-associated macrophages, regulatory T cells) in an AMPK-dependent manner[132,141]. Studies have also demonstrated that metformin can inhibit melanoma cell growth[142–144]. However, ongoing clinical trials continue to investigate metformin's anticancer role[141]. Beside metformin, another biguanide antidiabetic agent and mitochondrial complex I inhibitor, phenformin, is currently in clinical trials (NCT03026517) in combination with BRAF and MEK inhibitors for treating BRAF mutated melanomas[124,145,146].

Regarding the observation of the non-recurrent melanomas, tumor cells exhibit increased enrichment in pathways associated with extracellular matrix organization, collagen formation, coagulation, complement cascade, and mitophagy suggests a potential protective role against tumor recurrence. Particularly, mitophagy serves as a multifaceted defense mechanism in this context. During early tumorigenesis, it operates as a tumor suppressor by mitigating damage[147]. Moreover, by shielding against mitochondrial DNA mutations induced by ROS production, mitophagy may also diminish the occurrence of mtDNA mutations that contribute to cancer progression[147]. Consequently, the heightened enrichment of mitophagy in non-recurrent melanomas may indicate a more robust defense mechanism against tumor development. The increased enrichment of interleukin-related signaling pathways, collagen degradation, and the complement in the stromal cells of non-recurrent melanomas could potentially confer protection against tumor recurrence by enhancing immune responses against the tumor.

The relatively reduced abundance of proteins related to extracellular matrix organization, and immune response, including the complement and coagulation cascades in the recurrence group suggests a potential mechanism by which melanoma cells evade immune surveillance and progress. Prior studies have underscored the dysregulation of immune system-related pathways and immune cell infiltration in the tumor microenvironment, linking it with cancer progression and poor prognosis[126,127,148,149]. Conversely, the enrichment of mitochondrial translation, associated with melanoma development and progression[150], within the stromal cells of recurrent melanomas is intriguing, suggesting a potential transfer of the cancer cell phenotype to the microenvironment. In summary, our research reveals a unique molecular signature originating from both tumor and stromal cells of early-stage primary melanomas. These signatures could potentially predict the high risk of melanoma recurrence within a five-year timeframe.

To conclude our studies, these findings underscore the significance of proteins as predictive and prognostic targets identified from archived FFPE samples through IHC, quantitative proteomics and digital pathology with AI-driven imaging. These biomarkers offer insights into the molecular mechanisms underlying tumor cell-microenvironment interplay, therapy response variability in melanoma patients, and providing avenues for groundbreaking insights that could transform our understanding of melanoma's progression paving the way for personalized treatment strategies.

6. Summary, novel findings of the experimental work

In our discovery studies, we compared DNA-based PCR and protein-based IHC techniques to assess BRAF expression. Additionally, we applied new methodologies, including quantitative proteomics and AI-powered digital pathology, to identify predictive and prognostic proteins from formalin-fixed paraffin-embedded melanoma samples.

- Despite the rapid and cost-effective nature of IHC, significant discrepancies between BRAFV600E mutation detection by PCR and via IHC techniques highlighted the importance of the combined use of PCR and IHC, especially in cases of inhomogeneous and focal positive BRAF cases.

- At the first time, we were able to identify predictive proteins with deep proteomic sequencing from formalin-fixed paraffin-archived melanoma samples. The VEGFA-VEGFR2 pathway and RNA splicing pathways were connected to short progression-free survival, while increased activity of proteins and pathways from immune cells and extracellular matrix were associated with long progression-free survival in melanoma patients after the application of immunotherapy.

- For the first time, our findings revealed prognostic mechanisms from laser capture microdissected, formalin-fixed paraffin-embedded early-stage melanoma samples using quantitative proteomics and digital pathology with AI-driven imaging.

- We observed that upregulation of mitochondrial translation and cellular proliferation pathways, coupled with downregulation of immune response pathways, play pivotal roles in early-stage melanoma progression both in tumor and stromal cells.

In conclusion, diverse protein expression patterns observed across patient subgroups in our results suggest that immunohistochemistry, quantitative proteomics and digital pathology with AI-powered imaging, as aspects of spatial proteomics, are emerging, crucial technical components supporting therapy selection and precision medicine.

7. Acknowledgement

8. References

1. Saginala, K., Barsouk, A., Aluru, J.S., Rawla, P., and Barsouk, A. (2021). Epidemiology of Melanoma. Medical Sciences *9*, 63. https://doi.org/10.3390/medsci9040063.

2. Thomas, D., and Bello, D.M. (2021). Adjuvant immunotherapy for melanoma. Journal of Surgical Oncology *123*, 789–797. https://doi.org/10.1002/jso.26329.

3. Boussios, S., Rassy, E., Samartzis, E., Moschetta, M., Sheriff, M., Pérez-Fidalgo, J.A., and Pavlidis, N. (2021). Melanoma of unknown primary: New perspectives for an old story. Critical Reviews in Oncology/Hematology *158*, 103208. https://doi.org/10.1016/j.critrevonc.2020.103208.

4. Arnold, M., Singh, D., Laversanne, M., Vignat, J., Vaccarella, S., Meheus, F., Cust, A.E., De Vries, E., Whiteman, D.C., and Bray, F. (2022). Global Burden of Cutaneous Melanoma in 2020 and Projections to 2040. JAMA Dermatol *158*, 495. https://doi.org/10.1001/jamadermatol.2022.0160.

5. Kuras, M. (2023). Exploring the Complex and Multifaceted Interplay between Melanoma Cells and the Tumor Microenvironment. IJMS *24*, 14403. https://doi.org/10.3390/ijms241814403.

6. Naik, P.P. (2021). Cutaneous Malignant Melanoma: A Review of Early Diagnosis and Management. World J Oncol *12*, 7–19. https://doi.org/10.14740/wjon1349.

7. Lallier, T.E. (1991). Cell Lineage and Cell Migration in the Neural Crest. Annals of the New York Academy of Sciences *615*, 158–171. https://doi.org/10.1111/j.1749-6632.1991.tb37758.x.

8. Kollias, N., Sayre, R.M., Zeise, L., and Chedekel, M.R. (1991). New trends in photobiology. Journal of Photochemistry and Photobiology B: Biology *9*, 135–160. https://doi.org/10.1016/1011-1344(91)80147-A.

9. Raposo, G., and Marks, M.S. (2007). Melanosomes — dark organelles enlighten endosomal membrane transport. Nat Rev Mol Cell Biol *8*, 786–797. https://doi.org/10.1038/nrm2258.

10. Edited by Whitney A. High, MD, JD, MEng and Lori D. Prok, MD (2020). Dermatology Secrets, 6th Edition.

11. Garbe, C., Amaral, T., Peris, K., Hauschild, A., Arenberger, P., Bastholt, L., Bataille, V., Del Marmol, V., Dréno, B., Fargnoli, M.C., et al. (2020). European consensus-based interdisciplinary guideline for melanoma. Part 2: Treatment - Update 2019. Eur J Cancer *126*, 159–177. https://doi.org/10.1016/j.ejca.2019.11.015.

12. Gil, J., Betancourt, L.H., Pla, I., Sanchez, A., Appelqvist, R., Miliotis, T., Kuras, M., Oskolas, H., Kim, Y., Horvath, Z., et al. (2019). Clinical protein science in translational medicine targeting malignant melanoma. Cell Biol Toxicol *35*, 293–332. https://doi.org/10.1007/s10565-019-09468-6.

13. Mirna Situm, Marija Buljan 1, Maja Kolić, Majda Vučić Melanoma--clinical, dermatoscopical, and histopathological morphological characteristics. Acta Dermatovenerol Croat . https://doi.org/24813835.

14. Németh, I.B., Szadai, L., Jánosi, Á., Újfaludi, Z., Pankotai, T., Markó-Varga, G., Kemény, L., and Varga, E. (2022). The influence of molecular biology in the dermatopathology. BVSZ *98*, 152–158. https://doi.org/10.7188/bvsz.2022.98.3.7.

15. Gershenwald, J.E., and Scolyer, R.A. (2018). Melanoma Staging: American Joint Committee on Cancer (AJCC) 8th Edition and Beyond. Ann Surg Oncol *25*, 2105–2110. https://doi.org/10.1245/s10434-018-6513-7.

16. Sosman, J.A., Kim, K.B., Schuchter, L., Gonzalez, R., Pavlick, A.C., Weber, J.S., McArthur, G.A., Hutson, T.E., Moschos, S.J., Flaherty, K.T., et al. (2012). Survival in BRAF V600–Mutant Advanced Melanoma Treated with Vemurafenib. N Engl J Med *366*, 707–714. https://doi.org/10.1056/NEJMoa1112302.

17. Leslie, D., Lipsky, P., and Notkins, A.L. (2001). Autoantibodies as predictors of disease. J. Clin. Invest. *108*, 1417–1422. https://doi.org/10.1172/JCI14452.

18. Du Clos, T.W. (2000). Function of C-reactive protein. Annals of Medicine *32*, 274–278. https://doi.org/10.3109/07853890009011772.

19. Lilja, H., Ulmert, D., and Vickers, A.J. (2008). Prostate-specific antigen and prostate cancer: prediction, detection and monitoring. Nat Rev Cancer *8*, 268–278. https://doi.org/10.1038/nrc2351.

20. Peiris, A.N., Medlock, D., and Gavin, M. (2019). Thyroglobulin for Monitoring for Thyroid Cancer Recurrence. JAMA *321*, 1228. https://doi.org/10.1001/jama.2019.0803.

21. Ladányi, A., and Tímár, J. (2020). Immunologic and immunogenomic aspects of tumor progression. Seminars in Cancer Biology *60*, 249–261. https://doi.org/10.1016/j.semcancer.2019.08.011.

22. Zhang, T., Dutton-Regester, K., Brown, K.M., and Hayward, N.K. (2016). The genomic landscape of cutaneous melanoma. Pigment Cell Melanoma Res *29*, 266–283. https://doi.org/10.1111/pcmr.12459.

23. Tímár, J., and Ladányi, A. (2022). Molecular Pathology of Skin Melanoma: Epidemiology, Differential Diagnostics, Prognosis and Therapy Prediction. IJMS *23*, 5384. https://doi.org/10.3390/ijms23105384.

24. Valenti, F., Falcone, I., Ungania, S., Desiderio, F., Giacomini, P., Bazzichetto, C., Conciatori, F., Gallo, E., Cognetti, F., Ciliberto, G., et al. (2021). Precision Medicine and Melanoma: Multi-Omics Approaches to Monitoring the Immunotherapy Response. IJMS *22*, 3837. https://doi.org/10.3390/ijms22083837.

25. Rabbie, R., Ferguson, P., Molina-Aguilar, C., Adams, D.J., and Robles-Espinoza, C.D. (2019). Melanoma subtypes: genomic profiles, prognostic molecular markers and therapeutic possibilities. The Journal of Pathology *247*, 539–551. https://doi.org/10.1002/path.5213.

26. Erdag, G., Schaefer, J.T., Smolkin, M.E., Deacon, D.H., Shea, S.M., Dengel, L.T., Patterson, J.W., and Slingluff, C.L. (2012). Immunotype and Immunohistologic Characteristics of Tumor-Infiltrating Immune Cells Are Associated with Clinical Outcome in Metastatic Melanoma. Cancer Research *72*, 1070–1080. https://doi.org/10.1158/0008-5472.CAN-11-3218.

27. Cabrita, R., Lauss, M., Sanna, A., Donia, M., Skaarup Larsen, M., Mitra, S., Johansson, I., Phung, B., Harbst, K., Vallon-Christersson, J., et al. (2020). Tertiary lymphoid structures improve immunotherapy and survival in melanoma. Nature *577*, 561–565. https://doi.org/10.1038/s41586-019-1914-8.

28. Anwar, M.A.F., Murad, F., Dawson, E., Abd Elmageed, Z.Y., Tsumagari, K., and Kandil, E. (2016). Immunohistochemistry as a reliable method for detection of BRAF-V600E mutation in melanoma: a systematic review and meta-analysis of current published literature. Journal of Surgical Research *203*, 407–415. https://doi.org/10.1016/j.jss.2016.04.029.

29. Long, E., Ilie, M., Lassalle, S., Butori, C., Poissonnet, G., Washetine, K., Mouroux, J., Lespinet, V., Lacour, J.P., Taly, V., et al. (2015). Why and how immunohistochemistry should now be used to screen for the BRAFV 600E status in metastatic melanoma? The experience of a single institution (LCEP , Nice, France). Acad Dermatol Venereol *29*, 2436–2443. https://doi.org/10.1111/jdv.13332.

30. Schirosi, L., Strippoli, S., Gaudio, F., Graziano, G., Popescu, O., Guida, M., Simone, G., and Mangia, A. (2016). Is immunohistochemistry of BRAF V600E useful as a screening tool and

during progression disease of melanoma patients? BMC Cancer *16*, 905. https://doi.org/10.1186/s12885-016-2951-4.

31. Eckhart, L., Bach, J., Ban, J., and Tschachler, E. (2000). Melanin Binds Reversibly to Thermostable DNA Polymerase and Inhibits Its Activity. Biochemical and Biophysical Research Communications *271*, 726–730. https://doi.org/10.1006/bbrc.2000.2716.

32. Long-Mira, E., Picard-Gauci, A., Lassalle, S., Hofman, V., Lalvée, S., Tanga, V., Zahaf, K., Bonnetaud, C., Lespinet, V., Camuzard, O., et al. (2022). Comparison of Two Rapid Assays for the Detection of BRAF V600 Mutations in Metastatic Melanoma including Positive Sentinel Lymph Nodes. Diagnostics *12*, 751. https://doi.org/10.3390/diagnostics12030751.

33. Dávid Csaba Általános festési és immunhisztokémiai módszerek Makromolekulák azonosítása szövettani metszeteken.

34. Long, G.V., Wilmott, J.S., Capper, D., Preusser, M., Zhang, Y.E., Thompson, J.F., Kefford, R.F., Von Deimling, A., and Scolyer, R.A. (2013). Immunohistochemistry Is Highly Sensitive and Specific for the Detection of V600E BRAF Mutation in Melanoma. American Journal of Surgical Pathology *37*, 61–65. https://doi.org/10.1097/PAS.0b013e31826485c0.

35. Huang, W., Kuo, T., Wu, C., Cheng, H., Hsieh, C., Hsieh, J., Shen, Y., Hou, M., Hsu, T., and Chang, J.W. (2016). A comparison of immunohistochemical and molecular methods used for analyzing the *BRAF* V600E gene mutation in malignant melanoma in Taiwan. Asia-Pac J Clncl Oncology *12*, 403–408. https://doi.org/10.1111/ajco.12574.

36. Kuan, S.-F., Navina, S., Cressman, K.L., and Pai, R.K. (2014). Immunohistochemical detection of BRAF V600E mutant protein using the VE1 antibody in colorectal carcinoma is highly concordant with molecular testing but requires rigorous antibody optimization. Human Pathology *45*, 464–472. https://doi.org/10.1016/j.humpath.2013.10.026.

37. Gremel, G., Grannas, K., Sutton, L.A., Pontén, F., and Zieba, A. (2013). In situ Protein Detection for Companion Diagnostics. Front. Oncol. *3*. https://doi.org/10.3389/fonc.2013.00271.

38. Yarchoan, M., Albacker, L.A., Hopkins, A.C., Montesion, M., Murugesan, K., Vithayathil, T.T., Zaidi, N., Azad, N.S., Laheru, D.A., Frampton, G.M., et al. (2019). PD-L1 expression and tumor mutational burden are independent biomarkers in most cancers. JCI Insight *4*, e126908, 126908. https://doi.org/10.1172/jci.insight.126908.

39. Morrison, C., Pabla, S., Conroy, J.M., Nesline, M.K., Glenn, S.T., Dressman, D., Papanicolau-Sengos, A., Burgher, B., Andreas, J., Giamo, V., et al. (2018). Predicting response to checkpoint

inhibitors in melanoma beyond PD-L1 and mutational burden. J Immunother Cancer *6*, 32. https://doi.org/10.1186/s40425-018-0344-8.

40. Van Allen, E.M., Miao, D., Schilling, B., Shukla, S.A., Blank, C., Zimmer, L., Sucker, A., Hillen, U., Foppen, M.H.G., Goldinger, S.M., et al. (2015). Genomic correlates of response to CTLA-4 blockade in metastatic melanoma. Science *350*, 207–211. https://doi.org/10.1126/science.aad0095.

41. Addeo, A., Friedlaender, A., Banna, G.L., and Weiss, G.J. (2021). TMB or not TMB as a biomarker: That is the question. Critical Reviews in Oncology/Hematology *163*, 103374. https://doi.org/10.1016/j.critrevonc.2021.103374.

42. Marzagalli, M., Ebelt, N.D., and Manuel, E.R. (2019). Unraveling the crosstalk between melanoma and immune cells in the tumor microenvironment. Seminars in Cancer Biology *59*, 236–250. https://doi.org/10.1016/j.semcancer.2019.08.002.

43. Helmink, B.A., Reddy, S.M., Gao, J., Zhang, S., Basar, R., Thakur, R., Yizhak, K., Sade-Feldman, M., Blando, J., Han, G., et al. (2020). B cells and tertiary lymphoid structures promote immunotherapy response. Nature *577*, 549–555. https://doi.org/10.1038/s41586-019-1922-8.

44. Morrison, S.L., Han, G., Elenwa, F., Vetto, J.T., Fowler, G., Leong, S.P., Kashani-Sabet, M., Pockaj, B.A., Kosiorek, H.E., Zager, J.S., et al. (2022). Is the presence of tumor-infiltrating lymphocytes predictive of outcomes in patients with melanoma? Cancer *128*, 1418–1428. https://doi.org/10.1002/cncr.34013.

45. Antohe, M., Nedelcu, R., Nichita, L., Popp, C., Cioplea, M., Brinzea, A., Hodorogea, A., Calinescu, A., Balaban, M., Ion, D., et al. (2019). Tumor infiltrating lymphocytes: The regulator of melanoma evolution (Review). Oncol Lett. https://doi.org/10.3892/ol.2019.9940.

46. Kimm, M.A., Klenk, C., Alunni-Fabbroni, M., Kästle, S., Stechele, M., Ricke, J., Eisenblätter, M., and Wildgruber, M. (2021). Tumor-Associated Macrophages—Implications for Molecular Oncology and Imaging. Biomedicines *9*, 374. https://doi.org/10.3390/biomedicines9040374.

47. Carmen Phillips (2024). NIH: National Cancer Insititue: First Cancer TIL Therapy Gets FDA Approval for Advanced Melanoma. Cancer Currents Blog. https://www.cancer.gov/news-events/cancer-currents-blog/2024/fda-amtagvi-til-therapy-melanoma?fbclid=IwAR2QsZRGzlNnyKDwbchsKzSurSInL2jkeDq8w5AA9WRRc85WE1oXo z4jAds_aem_Aa0HVphvjarF8RL_2fz_NcHjFc_rvjutNXcg53xXu2fXusUwDCqIv_9oOylG-yTUIfGpbnS34-4_zkbfixNw-hGI.

48. Tan, W.C.C., Nerurkar, S.N., Cai, H.Y., Ng, H.H.M., Wu, D., Wee, Y.T.F., Lim, J.C.T., Yeong, J., and Lim, T.K.H. (2020). Overview of multiplex immunohistochemistry/immunofluorescence techniques in the era of cancer immunotherapy. Cancer Communications *40*, 135–153. https://doi.org/10.1002/cac2.12023.

49. Acs, B., Rantalainen, M., and Hartman, J. (2020). Artificial intelligence as the next step towards precision pathology. J Intern Med *288*, 62–81. https://doi.org/10.1111/joim.13030.

50. Acs, B., Ahmed, F.S., Gupta, S., Wong, P.F., Gartrell, R.D., Sarin Pradhan, J., Rizk, E.M., Gould Rothberg, B., Saenger, Y.M., and Rimm, D.L. (2019). An open source automated tumor infiltrating lymphocyte algorithm for prognosis in melanoma. Nat Commun *10*, 5440. https://doi.org/10.1038/s41467-019-13043-2.

51. Wan, G., Nguyen, N., Liu, F., DeSimone, M.S., Leung, B.W., Rajeh, A., Collier, M.R., Choi, M.S., Amadife, M., Tang, K., et al. (2022). Prediction of early-stage melanoma recurrence using clinical and histopathologic features. npj Precis. Onc. *6*, 79. https://doi.org/10.1038/s41698-022-00321-4.

52. Kulkarni, P.M., Robinson, E.J., Sarin Pradhan, J., Gartrell-Corrado, R.D., Rohr, B.R., Trager, M.H., Geskin, L.J., Kluger, H.M., Wong, P.F., Acs, B., et al. (2020). Deep Learning Based on Standard H&E Images of Primary Melanoma Tumors Identifies Patients at Risk for Visceral Recurrence and Death. Clinical Cancer Research *26*, 1126–1134. https://doi.org/10.1158/1078-0432.CCR-19-1495.

53. Lapuente-Santana, Ó., van Genderen, M., Hilbers, P.A.J., Finotello, F., and Eduati, F. (2021). Interpretable systems biomarkers predict response to immune-checkpoint inhibitors. Patterns (N Y) *2*, 100293. https://doi.org/10.1016/j.patter.2021.100293.

54. The Human Protein Atlas - ITGAX (2023). https://www.proteinatlas.org/ENSG00000140678-ITGAX https://www.proteinatlas.org/ENSG00000140678-ITGAX.

55. The Human Protein Atlas – SAMSN1. (2023). https://www.proteinatlas.org/ENSG00000155307-SAMSN1 https://www.proteinatlas.org/ENSG00000155307-SAMSN1.

56. Jia, L., Shi, Y., Wen, Y., Li, W., Feng, J., and Chen, C. (2018). The roles of TNFAIP2 in cancers and infectious diseases. J Cell Mol Med *22*, 5188–5195. https://doi.org/10.1111/jcmm.13822.

57. The Human Protein Atlas – TNFAIP2. (2023).
    https://www.proteinatlas.org/ENSG00000185215-TNFAIP2/
    https://www.proteinatlas.org/ENSG00000185215-TNFAIP2/.

58. The Human Protein Atlas – CD163 (2023). https://www.proteinatlas.org/ENSG00000177575-
    CD163/ https://www.proteinatlas.org/ENSG00000177575-CD163/.

59. Huang, Y., Lemire, G., Briere, L.C., Liu, F., Wessels, M.W., Wang, X., Osmond, M., Kanca, O.,
    Lu, S., High, F.A., et al. (2022). The recurrent de novo c.2011C>T missense variant in MTSS2
    causes syndromic intellectual disability. Am J Hum Genet *109*, 1923–1931.
    https://doi.org/10.1016/j.ajhg.2022.08.011.

60. Szadai, L., Bartha, A., Parada, I.P., Lakatos, A.I.T., Pál, D.M.P., Lengyel, A.S., de Almeida,
    N.P., Jánosi, Á.J., Nogueira, F., Szeitz, B., et al. (2024). Predicting immune checkpoint therapy
    response in three independent metastatic melanoma cohorts. Frontiers in Oncology *14*.

61. Velasquez, E., Szadai, L., Zhou, Q., Kim, Y., Pla, I., Sanchez, A., Appelqvist, R., Oskolas, H.,
    Marko-Varga, M., Lee, B., et al. (2021). A biobanking turning-point in the use of formalin-fixed,
    paraffin tumor blocks to unveil kinase signaling in melanoma. Clinical & Translational Med *11*,
    e466. https://doi.org/10.1002/ctm2.466.

62. Betancourt, L.H., Gil, J., Sanchez, A., Doma, V., Kuras, M., Murillo, J.R., Velasquez, E., Çakır,
    U., Kim, Y., Sugihara, Y., et al. (2021). The Human Melanoma Proteome Atlas-Complementing
    the melanoma transcriptome. Clin Transl Med *11*, e451. https://doi.org/10.1002/ctm2.451.

63. Betancourt, L.H., Gil, J., Kim, Y., Doma, V., Çakır, U., Sanchez, A., Murillo, J.R., Kuras, M.,
    Parada, I.P., Sugihara, Y., et al. (2021). The human melanoma proteome atlas-Defining the
    molecular pathology. Clin Transl Med *11*, e473. https://doi.org/10.1002/ctm2.473.

64. Szadai, L., Velasquez, E., Szeitz, B., Almeida, N.P. de, Domont, G., Betancourt, L.H., Gil, J.,
    Marko-Varga, M., Oskolas, H., Jánosi, Á.J., et al. (2021). Deep Proteomic Analysis on
    Biobanked Paraffine-Archived Melanoma with Prognostic/Predictive Biomarker Read-Out.
    Cancers (Basel) *13*, 6105. https://doi.org/10.3390/cancers13236105.

65. Pirhonen, J., Szkalisity, Á., Hagström, J., Kim, Y., Migh, E., Kovács, M., Hölttä, M., Peränen, J.,
    Seppänen, H., Haglund, C., et al. (2022). Lipid Metabolic Reprogramming Extends beyond
    Histologic Tumor Demarcations in Operable Human Pancreatic Cancer. Cancer Research *82*,
    3932–3949. https://doi.org/10.1158/0008-5472.CAN-22-0396.

66. Szadai, L., Guedes, J.D.S., Woldmar, N., De Almeida, N.P., Jánosi, Á.J., Rajeh, A., Kovács, F., Kriston, A., Migh, E., Wan, G., et al. (2023). Mitochondrial and immune response dysregulation in melanoma recurrence. Clinical & Translational Med *13*, e1495. https://doi.org/10.1002/ctm2.1495.

67. Priskin, K., Pólya, S., Pintér, L., Jaksa, G., Csányi, B., Enyedi, M.Z., Sági-Zsigmond, E., Sükösd, F., Oláh-Németh, O., Kelemen, G., et al. (2021). BC-Monitor: Towards a Routinely Accessible Circulating Tumor DNA-Based Tool for Real-Time Monitoring Breast Cancer Progression and Treatment Effectiveness. Cancers *13*, 3489. https://doi.org/10.3390/cancers13143489.

68. Edgar, R.C., and Flyvbjerg, H. (2015). Error filtering, pair assembly and error correction for next-generation sequencing reads. Bioinformatics *31*, 3476–3482. https://doi.org/10.1093/bioinformatics/btv401.

69. Smith, T., Heger, A., and Sudbery, I. (2017). UMI-tools: modeling sequencing errors in Unique Molecular Identifiers to improve quantification accuracy. Genome Res. *27*, 491–499. https://doi.org/10.1101/gr.209601.116.

70. Mund, A., Coscia, F., Kriston, A., Hollandi, R., Kovács, F., Brunner, A.-D., Migh, E., Schweizer, L., Santos, A., Bzorek, M., et al. (2022). Deep Visual Proteomics defines single-cell identity and heterogeneity. Nat Biotechnol *40*, 1231–1240. https://doi.org/10.1038/s41587-022-01302-5.

71. Hollandi, R., Szkalisity, A., Toth, T., Tasnadi, E., Molnar, C., Mathe, B., Grexa, I., Molnar, J., Balind, A., Gorbe, M., et al. (2020). nucleAIzer: A Parameter-free Deep Learning Framework for Nucleus Segmentation Using Image Style Transfer. Cell Systems *10*, 453-458.e6. https://doi.org/10.1016/j.cels.2020.04.003.

72. Kuras, M., Woldmar, N., Kim, Y., Hefner, M., Malm, J., Moldvay, J., Döme, B., Fillinger, J., Pizzatti, L., Gil, J., et al. (2021). Proteomic Workflows for High-Quality Quantitative Proteome and Post-Translational Modification Analysis of Clinically Relevant Samples from Formalin-Fixed Paraffin-Embedded Archives. J. Proteome Res. *20*, 1027–1039. https://doi.org/10.1021/acs.jproteome.0c00850.

73. Cˇ uklina, J. (2018). Computational Challenges in Biomarker Discovery from High-Throughput Proteomic Data. Ph.D. Thesis.

74. Tyanova, S., and Cox, J. (2018). Perseus: A Bioinformatics Platform for Integrative Analysis of Proteomics Data in Cancer Research. In Cancer Systems Biology Methods in Molecular

Biology., L. Von Stechow, ed. (Springer New York), pp. 133–148. https://doi.org/10.1007/978-1-4939-7493-1_7.

75. SPSS 27 Software (SPSS Inc,).

76. RStudio v. 1.4.1106 https://global.rstudio.com/products/rstudio/older-versions/ https://global.rstudio.com/products/rstudio/older-versions/.

77. Wickham, H. (2016). ggplot2 Elegant Graphics for Data Analysis (New York: Springer-Verlag).

78. Vu, V. Ggbiplot. https://github.com/vqv/ggbiplot https://github.com/vqv/ggbiplot.

79. Wilke, C.O. Cowplot:Streamlined Plot Theme and Plot Annotations for "Ggplot2. https://CRAN.R-project. org/package=cowplot https://CRAN.R-project. org/package=cowplot.

80. Auguie, B.; Antonov, A. GridExtra: Miscellaneous Functions for "Grid" Graphics. https://CRAN.R-project. org/package=gridExtra https://CRAN.R-project. org/package=gridExtra.

81. Gu, Z., Eils, R., and Schlesner, M. (2016). Complex heatmaps reveal patterns and correlations in multidimensional genomic data. Bioinformatics *32*, 2847–2849. https://doi.org/10.1093/bioinformatics/btw313.

82. Szklarczyk, D., Gable, A.L., Nastou, K.C., Lyon, D., Kirsch, R., Pyysalo, S., Doncheva, N.T., Legeay, M., Fang, T., Bork, P., et al. (2021). The STRING database in 2021: customizable protein–protein networks, and functional characterization of user-uploaded gene/measurement sets. Nucleic Acids Research *49*, D605–D612. https://doi.org/10.1093/nar/gkaa1074.

83. Shannon, P., Markiel, A., Ozier, O., Baliga, N.S., Wang, J.T., Ramage, D., Amin, N., Schwikowski, B., and Ideker, T. (2003). Cytoscape: A Software Environment for Integrated Models of Biomolecular Interaction Networks. Genome Res. *13*, 2498–2504. https://doi.org/10.1101/gr.1239303.

84. The Gene Ontology Consortium, Carbon, S., Douglass, E., Good, B.M., Unni, D.R., Harris, N.L., Mungall, C.J., Basu, S., Chisholm, R.L., Dodson, R.J., et al. (2021). The Gene Ontology resource: enriching a GOld mine. Nucleic Acids Research *49*, D325–D334. https://doi.org/10.1093/nar/gkaa1113.

85. Kanehisa, M. (2000). KEGG: Kyoto Encyclopedia of Genes and Genomes. Nucleic Acids Research *28*, 27–30. https://doi.org/10.1093/nar/28.1.27.

86. Graphpad Prism 9 (2024). https://www.graphpad.com/updates/prism-900-release-notes https://www.graphpad.com/updates/prism-900-release-notes.

87. Subramanian, A., Tamayo, P., Mootha, V.K., Mukherjee, S., Ebert, B.L., Gillette, M.A., Paulovich, A., Pomeroy, S.L., Golub, T.R., Lander, E.S., et al. (2005). Gene set enrichment analysis: A knowledge-based approach for interpreting genome-wide expression profiles. Proc. Natl. Acad. Sci. U.S.A. *102*, 15545–15550. https://doi.org/10.1073/pnas.0506580102.

88. Liberzon, A., Subramanian, A., Pinchback, R., Thorvaldsdóttir, H., Tamayo, P., and Mesirov, J.P. (2011). Molecular signatures database (MSigDB) 3.0. Bioinformatics *27*, 1739–1740. https://doi.org/10.1093/bioinformatics/btr260.

89. Jassal, B., Matthews, L., Viteri, G., Gong, C., Lorente, P., Fabregat, A., Sidiropoulos, K., Cook, J., Gillespie, M., Haw, R., et al. (2019). The reactome pathway knowledgebase. Nucleic Acids Research, gkz1031. https://doi.org/10.1093/nar/gkz1031.

90. Biorender (2024).

91. Yancovitz, M., Litterman, A., Yoon, J., Ng, E., Shapiro, R.L., Berman, R.S., Pavlick, A.C., Darvishian, F., Christos, P., Mazumdar, M., et al. (2012). Intra- and Inter-Tumor Heterogeneity of BRAFV600EMutations in Primary and Metastatic Melanoma. PLoS ONE *7*, e29336. https://doi.org/10.1371/journal.pone.0029336.

92. Katona, D. (2021). Mutáció specifikus BRAFV600E immunhisztokémia humán melanoma szöveten.

93. Maley, C.C., Galipeau, P.C., Finley, J.C., Wongsurawat, V.J., Li, X., Sanchez, C.A., Paulson, T.G., Blount, P.L., Risques, R.-A., Rabinovitch, P.S., et al. (2006). Genetic clonal diversity predicts progression to esophageal adenocarcinoma. Nat Genet *38*, 468–473. https://doi.org/10.1038/ng1768.

94. Liegl, B., Kepten, I., Le, C., Zhu, M., Demetri, G., Heinrich, M., Fletcher, C., Corless, C., and Fletcher, J. (2008). Heterogeneity of kinase inhibitor resistance mechanisms in GIST. The Journal of Pathology *216*, 64–74. https://doi.org/10.1002/path.2382.

95. Taniguchi, K., Okami, J., Kodama, K., Higashiyama, M., and Kato, K. (2008). Intratumor heterogeneity of epidermal growth factor receptor mutations in lung cancer and its correlation to the response to gefitinib. Cancer Science *99*, 929–935. https://doi.org/10.1111/j.1349-7006.2008.00782.x.

96. Menzies, A.M., Lum, T., Wilmott, J.S., Hyman, J., Kefford, R.F., Thompson, J.F., O'Toole, S., Long, G.V., and Scolyer, R.A. (2014). Intrapatient Homogeneity of BRAFV600E Expression in Melanoma. American Journal of Surgical Pathology *38*, 377–382. https://doi.org/10.1097/PAS.0000000000000136.

97. Ihle, M.A., Fassunke, J., König, K., Grünewald, I., Schlaak, M., Kreuzberg, N., Tietze, L., Schildhaus, H.-U., Büttner, R., and Merkelbach-Bruse, S. (2014). Comparison of high resolution melting analysis, pyrosequencing, next generation sequencing and immunohistochemistry to conventional Sanger sequencing for the detection of p.V600E and non-p.V600E BRAFmutations. BMC Cancer *14*, 13. https://doi.org/10.1186/1471-2407-14-13.

98. Tímár, J., Vizkeleti, L., Doma, V., Barbai, T., and Rásó, E. (2016). Genetic progression of malignant melanoma. Cancer Metastasis Rev *35*, 93–107. https://doi.org/10.1007/s10555-016-9613-5.

99. Alessi, C., Scapulatempo Neto, C., Viana, C.R., and Vazquez, V.D.L. (2017). PD-1/PD-L1 and VEGF-A/VEGF-C expression in lymph node microenvironment and association with melanoma metastasis and survival. Melanoma Research *27*, 565–572. https://doi.org/10.1097/CMR.0000000000000396.

100. Frezzetti, D., Gallo, M., Maiello, M.R., D'Alessio, A., Esposito, C., Chicchinelli, N., Normanno, N., and De Luca, A. (2017). VEGF as a potential target in lung cancer. Expert Opinion on Therapeutic Targets *21*, 959–966. https://doi.org/10.1080/14728222.2017.1371137.

101. Ferrara, N., Hillan, K.J., and Novotny, W. (2005). Bevacizumab (Avastin), a humanized anti-VEGF monoclonal antibody for cancer therapy. Biochemical and Biophysical Research Communications *333*, 328–335. https://doi.org/10.1016/j.bbrc.2005.05.132.

102. NOS3 Protein Expression Summary—The Human Protein Atlas https://www.proteinatlas.org/ENSG00000164867-NOS3 https://www.proteinatlas.org/ENSG00000164867-NOS3.

103. Melo, F.H.M.D., Gonçalves, D.A., Sousa, R.X.D., Icimoto, M.Y., Fernandes, D.D.C., Laurindo, F.R.M., and Jasiulionis, M.G. (2021). Metastatic Melanoma Progression Is Associated with Endothelial Nitric Oxide Synthase Uncoupling Induced by Loss of eNOS:BH4 Stoichiometry. IJMS *22*, 9556. https://doi.org/10.3390/ijms22179556.

104. Deng, K., Yao, J., Huang, J., Ding, Y., and Zuo, J. (2021). Abnormal alternative splicing promotes tumor resistance in targeted therapy and immunotherapy. Translational Oncology *14*, 101077. https://doi.org/10.1016/j.tranon.2021.101077.

105. Eymin, B. (2021). Targeting the spliceosome machinery: A new therapeutic axis in cancer? Biochemical Pharmacology *189*, 114039. https://doi.org/10.1016/j.bcp.2020.114039.

106. Effenberger, K.A., Urabe, V.K., and Jurica, M.S. (2017). Modulating splicing with small molecular inhibitors of the spliceosome. WIREs RNA *8*, e1381. https://doi.org/10.1002/wrna.1381.

107. Babačić, H., Lehtiö, J., Pico De Coaña, Y., Pernemalm, M., and Eriksson, H. (2020). In-depth plasma proteomics reveals increase in circulating PD-1 during anti-PD-1 immunotherapy in patients with metastatic cutaneous melanoma. J Immunother Cancer *8*, e000204. https://doi.org/10.1136/jitc-2019-000204.

108. The Human Protein Atlas: Purine nucleoside phosphorylase - protein summary. https://www.proteinatlas.org/ENSG00000198805-PNP https://www.proteinatlas.org/ENSG00000198805-PNP.

109. Bantia, S. (2015). Purine nucleoside phosphorylase inhibitors - an immunotherapy with novel mechanism of action for the treatment of melanoma. j. immunotherapy cancer *3*, P292, 2051-1426-3-S2-P292. https://doi.org/10.1186/2051-1426-3-S2-P292.

110. Shanta, B. (2020). Purine Nucleoside Phosphorylase Inhibitors as Novel Immuno-Oncology Agent and Vaccine Adjuvant. Int J Immunol Immunother *7*. https://doi.org/10.23937/2378-3672/1410043.

111. The Human Protein Atlas: Ferritin heavy chain 1 - protein summary. https://www.proteinatlas.org/ENSG00000167996-FTH1 https://www.proteinatlas.org/ENSG00000167996-FTH1.

112. Shi, X., Zhang, A., Lu, J., Wang, X., Yi, C., and Yang, F. (2023). An Overview of Heavy Chain Ferritin in Cancer. Front. Biosci. (Landmark Ed) *28*, 182. https://doi.org/10.31083/j.fbl2808182.

113. Gray CP, Arosio P, Hersey P. Association of increased levels of heavy-chain ferritin with increased CD4+ CD25+ regulatory T-cell levels in patients with melanoma. Clin Cancer Res.

114. Wang, K., Xuan, Z., Liu, X., Zheng, M., Yang, C., and Wang, H. (2022). Immunomodulatory role of metalloproteinase ADAM17 in tumor development. Front. Immunol. *13*, 1059376. https://doi.org/10.3389/fimmu.2022.1059376.

115. Andrews, L.P., Somasundaram, A., Moskovitz, J.M., Szymczak-Workman, A.L., Liu, C., Cillo, A.R., Lin, H., Normolle, D.P., Moynihan, K.D., Taniuchi, I., et al. (2020). Resistance to PD1

blockade in the absence of metalloprotease-mediated LAG3 shedding. Sci Immunol *5*, eabc2728. https://doi.org/10.1126/sciimmunol.abc2728.

116. Huang, L., Chen, J., Quan, J., and Xiang, D. (2021). Rosmarinic acid inhibits proliferation and migration, promotes apoptosis and enhances cisplatin sensitivity of melanoma cells through inhibiting ADAM17/EGFR/AKT/GSK3β axis. Bioengineered *12*, 3065–3076. https://doi.org/10.1080/21655979.2021.1941699.

117. Fejza, A., Polano, M., Camicia, L., Poletto, E., Carobolante, G., Toffoli, G., Mongiat, M., and Andreuzzi, E. (2021). The Efficacy of Anti-PD-L1 Treatment in Melanoma Is Associated with the Expression of the ECM Molecule EMILIN2. IJMS *22*, 7511. https://doi.org/10.3390/ijms22147511.

118. Wang, H., Pan, J., Barsky, L., Jacob, J.C., Zheng, Y., Gao, C., Wang, S., Zhu, W., Sun, H., Lu, L., et al. (2021). Characteristics of pre-metastatic niche: the landscape of molecular and cellular pathways. Mol Biomed *2*, 3. https://doi.org/10.1186/s43556-020-00022-z.

119. Simonaggio, A., Epaillard, N., Pobel, C., Moreira, M., Oudard, S., and Vano, Y.-A. (2021). Tumor Microenvironment Features as Predictive Biomarkers of Response to Immune Checkpoint Inhibitors (ICI) in Metastatic Clear Cell Renal Cell Carcinoma (mccRCC). Cancers *13*, 231. https://doi.org/10.3390/cancers13020231.

120. Huang, C., Radi, R.H., and Arbiser, J.L. (2021). Mitochondrial Metabolism in Melanoma. Cells *10*, 3197. https://doi.org/10.3390/cells10113197.

121. Kunji, E.R.S., Aleksandrova, A., King, M.S., Majd, H., Ashton, V.L., Cerson, E., Springett, R., Kibalchenko, M., Tavoulari, S., Crichton, P.G., et al. (2016). The transport mechanism of the mitochondrial ADP/ATP carrier. Biochimica et Biophysica Acta (BBA) - Molecular Cell Research *1863*, 2379–2393. https://doi.org/10.1016/j.bbamcr.2016.03.015.

122. Jiang, T., Zhuang, J., Duan, H., Luo, Y., Zeng, Q., Fan, K., Yan, H., Lu, D., Ye, Z., Hao, J., et al. (2012). CD146 is a coreceptor for VEGFR-2 in tumor angiogenesis. Blood *120*, 2330–2339. https://doi.org/10.1182/blood-2012-01-406108.

123. David, C.J., Chen, M., Assanah, M., Canoll, P., and Manley, J.L. (2010). HnRNP proteins controlled by c-Myc deregulate pyruvate kinase mRNA splicing in cancer. Nature *463*, 364–368. https://doi.org/10.1038/nature08697.

124. Natália Pinto de Almeida, Ágnes Judit Jánosi, Runyu Hong, Ahmad Rajeh, Fábio Nogueira, Leticia Szadai, Beata Szeitz, Indira Pla Parada, Viktória Doma, Nicole Woldmar, Jéssica

Guedes, Zsuzsanna Újfaludi, Aron Bartha, Yonghyo Kim, Charlotte Welinder, Bo Baldetorp, Lajos Vince Kemény, Zoltan Pahi, Guihong Wan, Nga Nguyen, Tibor Pankotai, Balázs Győrffy, Krzysztof Pawłowski, Peter Horvatovich, Attila Marcell Szasz, Aniel Sanchez, Magdalena Kuras, Jimmy Rodriguez Murillo, Lazaro Betancourt, Gilberto B. Domont, Yevgeniy R. Semenov, Kun-Hsing Yu, Ho Jeong Kwon, István Balázs Németh, David Fenyő, Elisabet Wieslander, György Marko-Varga, Jeovanis Gil (2024). Mitochondrial dysfunction and immune suppression in BRAF V600E-mutated metastatic melanoma. *Volume14, Issue7, July 2024, e1773*. https://doi.org/10.1002/ctm2.1773.

125. Delgado-Goñi, T., Galobart, T.C., Wantuch, S., Normantaite, D., Leach, M.O., Whittaker, S.R., and Beloueche-Babari, M. (2020). Increased inflammatory lipid metabolism and anaplerotic mitochondrial activation follow acquired resistance to vemurafenib in BRAF-mutant melanoma cells. Br J Cancer *122*, 72–81. https://doi.org/10.1038/s41416-019-0628-x.

126. Li, C., Xu, X., Wei, S., Jiang, P., Xue, L., and Wang, J. (2021). Tumor-associated macrophages: potential therapeutic strategies and future prospects in cancer. J Immunother Cancer *9*, e001341. https://doi.org/10.1136/jitc-2020-001341.

127. Jin, S., Li, R., Chen, M.-Y., Yu, C., Tang, L.-Q., Liu, Y.-M., Li, J.-P., Liu, Y.-N., Luo, Y.-L., Zhao, Y., et al. (2020). Single-cell transcriptomic analysis defines the interplay between tumor cells, viral infection, and the microenvironment in nasopharyngeal carcinoma. Cell Res *30*, 950–965. https://doi.org/10.1038/s41422-020-00402-8.

128. Avagliano, A., Fiume, G., Pelagalli, A., Sanità, G., Ruocco, M.R., Montagnani, S., and Arcucci, A. (2020). Metabolic Plasticity of Melanoma Cells and Their Crosstalk With Tumor Microenvironment. Front. Oncol. *10*, 722. https://doi.org/10.3389/fonc.2020.00722.

129. Luís, R., Brito, C., and Pojo, M. (2020). Melanoma Metabolism: Cell Survival and Resistance to Therapy. In Tumor Microenvironment Advances in Experimental Medicine and Biology., J. Serpa, ed. (Springer International Publishing), pp. 203–223. https://doi.org/10.1007/978-3-030-34025-4_11.

130. Gil, J., Kim, Y., Doma, V., Çakır, U., Kuras, M., Betancourt, L.H., Parada, I.P., Sanchez, A., Sugihara, Y., Appelqvist, R., et al. (2022). Proteogenomic Characterization Reveals Therapeutic Opportunities Related to Mitochondrial Function in Melanoma. Preprint, https://doi.org/10.1101/2022.10.24.513481 https://doi.org/10.1101/2022.10.24.513481.

131. Feng, J., Wang, X., Ye, X., Ares, I., Lopez-Torres, B., Martínez, M., Martínez-Larrañaga, M.-R., Wang, X., Anadón, A., and Martínez, M.-A. (2022). Mitochondria as an important target of

metformin: The mechanism of action, toxic and side effects, and new therapeutic applications. Pharmacological Research *177*, 106114. https://doi.org/10.1016/j.phrs.2022.106114.

132. Gupta, J., Jalil, A.T., Abd Alzahraa, Z.H., Aminov, Z., Alsaikhan, F., Ramírez-Coronel, A.A., Ramaiah, P., and Najafi, M. (2023). The metformin immunoregulatory actions in tumor suppression and normal tissues protection. CMC *31*. https://doi.org/10.2174/0929867331666230703143907.

133. Gui, D.Y., Sullivan, L.B., Luengo, A., Hosios, A.M., Bush, L.N., Gitego, N., Davidson, S.M., Freinkman, E., Thomas, C.J., and Vander Heiden, M.G. (2016). Environment Dictates Dependence on Mitochondrial Complex I for NAD+ and Aspartate Production and Determines Cancer Cell Sensitivity to Metformin. Cell Metabolism *24*, 716–727. https://doi.org/10.1016/j.cmet.2016.09.006.

134. Cheng, G., Zielonka, J., Ouari, O., Lopez, M., McAllister, D., Boyle, K., Barrios, C.S., Weber, J.J., Johnson, B.D., Hardy, M., et al. (2016). Mitochondria-Targeted Analogues of Metformin Exhibit Enhanced Antiproliferative and Radiosensitizing Effects in Pancreatic Cancer Cells. Cancer Research *76*, 3904–3915. https://doi.org/10.1158/0008-5472.CAN-15-2534.

135. Sancho, P., Burgos-Ramos, E., Tavera, A., Bou Kheir, T., Jagust, P., Schoenhals, M., Barneda, D., Sellers, K., Campos-Olivas, R., Graña, O., et al. (2015). MYC/PGC-1α Balance Determines the Metabolic Phenotype and Plasticity of Pancreatic Cancer Stem Cells. Cell Metabolism *22*, 590–605. https://doi.org/10.1016/j.cmet.2015.08.015.

136. Boyle, K.A., Van Wickle, J., Hill, R.B., Marchese, A., Kalyanaraman, B., and Dwinell, M.B. (2018). Mitochondria-targeted drugs stimulate mitophagy and abrogate colon cancer cell proliferation. Journal of Biological Chemistry *293*, 14891–14904. https://doi.org/10.1074/jbc.RA117.001469.

137. Verdura, S., Cuyàs, E., Martin-Castillo, B., and Menendez, J.A. (2019). Metformin as an archetype immuno-metabolic adjuvant for cancer immunotherapy. OncoImmunology *8*, e1633235. https://doi.org/10.1080/2162402X.2019.1633235.

138. Vancura, A., Bu, P., Bhagwat, M., Zeng, J., and Vancurova, I. (2018). Metformin as an Anticancer Agent. Trends in Pharmacological Sciences *39*, 867–878. https://doi.org/10.1016/j.tips.2018.07.006.

139. Cha, J.-H., Yang, W.-H., Xia, W., Wei, Y., Chan, L.-C., Lim, S.-O., Li, C.-W., Kim, T., Chang, S.-S., Lee, H.-H., et al. (2018). Metformin Promotes Antitumor Immunity via Endoplasmic-

Reticulum-Associated Degradation of PD-L1. Molecular Cell *71*, 606-620.e7. https://doi.org/10.1016/j.molcel.2018.07.030.

140. Dreher, L.-S., and Hoppe, T. (2018). ERADicate Tumor Progression with Metformin. Molecular Cell *71*, 481–482. https://doi.org/10.1016/j.molcel.2018.08.001.

141. Galal, M.A., Al-Rimawi, M., Hajeer, A., Dahman, H., Alouch, S., and Aljada, A. (2024). Metformin: A Dual-Role Player in Cancer Treatment and Prevention. IJMS *25*, 4083. https://doi.org/10.3390/ijms25074083.

142. Li, K., Zhang, T., Wang, F., Cui, B., Zhao, C., Yu, J., Lv, X., Zhang, X., Yang, Z., Huang, B., et al. (2018). Metformin suppresses melanoma progression by inhibiting KAT5-mediated SMAD3 acetylation, transcriptional activity and TRIB3 expression. Oncogene *37*, 2967–2981. https://doi.org/10.1038/s41388-018-0172-9.

143. Tomic, T., Botton, T., Cerezo, M., Robert, G., Luciano, F., Puissant, A., Gounon, P., Allegra, M., Bertolotto, C., Bereder, J.-M., et al. (2011). Metformin inhibits melanoma development through autophagy and apoptosis mechanisms. Cell Death Dis *2*, e199–e199. https://doi.org/10.1038/cddis.2011.86.

144. Petti, C., Vegetti, C., Molla, A., Bersani, I., Cleris, L., Mustard, K.J., Formelli, F., Hardie, G.D., Sensi, M., and Anichini, A. (2012). AMPK activators inhibit the proliferation of human melanomas bearing the activated MAPK pathway. Melanoma Research *22*, 341–350. https://doi.org/10.1097/CMR.0b013e3283544929.

145. Chapman, P.B., Klang, M., Postow, M.A., Shoushtari, A.N., Sullivan, R.J., Wolchok, J.D., Wong, P., Callahan, M.K., and Zippin, J. (2023). Targeting AMP kinase in melanoma: A phase I trial of phenformin with dabrafenib/trametinib. JCO *41*, 9536–9536. https://doi.org/10.1200/JCO.2023.41.16_suppl.9536.

146. Yuan, P., Ito, K., Perez-Lorenzo, R., Del Guzzo, C., Lee, J.H., Shen, C.-H., Bosenberg, M.W., McMahon, M., Cantley, L.C., and Zheng, B. (2013). Phenformin enhances the therapeutic benefit of BRAF ^{V600E} inhibition in melanoma. Proc. Natl. Acad. Sci. U.S.A. *110*, 18226–18231. https://doi.org/10.1073/pnas.1317577110.

147. Li, L., and Hu, F. (2023). Mitophagy in tumor: foe or friend？. Endokrynol Pol *74*, 511–519. https://doi.org/10.5603/ep.95652.

148. Rømer, A.M.A., Thorseth, M.-L., and Madsen, D.H. (2021). Immune Modulatory Properties of Collagen in Cancer. Front. Immunol. *12*, 791453. https://doi.org/10.3389/fimmu.2021.791453.

149. Chen, Y., Feng, Y., Yan, F., Zhao, Y., Zhao, H., and Guo, Y. (2022). A Novel Immune-Related Gene Signature to Identify the Tumor Microenvironment and Prognose Disease Among Patients With Oral Squamous Cell Carcinoma Patients Using ssGSEA: A Bioinformatics and Biological Validation Study. Front. Immunol. *13*, 922195. https://doi.org/10.3389/fimmu.2022.922195.

150. Gil, J., Rezeli, M., Lutz, E.G., Kim, Y., Sugihara, Y., Malm, J., Semenov, Y.R., Yu, K.-H., Nguyen, N., Wan, G., et al. (2021). An Observational Study on the Molecular Profiling of Primary Melanomas Reveals a Progression Dependence on Mitochondrial Activation. Cancers *13*, 6066. https://doi.org/10.3390/cancers13236066.